Journal Pre-proof

Source and deposition age of the Dialé-Daléma metasedimentary series (Kédougou-Kéniéba Inlier, Senegal) constrained by U–Pb geochronology on detrital zircon grains

J. Kone, O. Vanderhaeghe, F. Diatta, L. Baratoux, N. Thebaud, O. Bruguier, P.M. Ndiaye, S. Duchene, P. Pitra, J. Ganne

PII: S1464-343X(20)30052-2

DOI: https://doi.org/10.1016/j.jafrearsci.2020.103801

Reference: AES 103801

To appear in: *Journal of African Earth Sciences*

Received Date: 20 August 2019

Revised Date: 18 January 2020

Accepted Date: 18 February 2020

Please cite this article as: Kone, J., Vanderhaeghe, O., Diatta, F., Baratoux, L., Thebaud, N., Bruguier, O., Ndiaye, P.M., Duchene, S., Pitra, P., Ganne, J., Source and deposition age of the Dialé-Daléma metasedimentary series (Kédougou-Kéniéba Inlier, Senegal) constrained by U–Pb geochronology on detrital zircon grains, *Journal of African Earth Sciences* (2020), doi: https://doi.org/10.1016/j.jafrearsci.2020.103801.

Source and deposition age of the Dialé-Daléma metasedimentary series (Kédougou-Kéniéba Inlier, Senegal) constrained by U-Pb geochronology on detrital zircon grains

J. KONE [1,2], O. VANDERHAEGHE [2], F. DIATTA [3], L. BARATOUX [1,2], N. THEBAUD [4], O. BRUGUIER [5], P.M. NDIAYE [3], S. DUCHENE [2], P. PITRA [6,7], J. GANNE [2]

[1]*IFAN, Cheikh Anta Diop, Dakar, Sénégal.*

[2]*Geosciences Environnement Toulouse, Observatoire Midi Pyrénées, UPS, CNRS, IRD, 14 avenue E. Belin, 31400 Toulouse, France.*

[3]*Département de Géologie, Université Cheikh Anta Diop, Dakar, Sénégal.*

[4]*Centre for Exploration Targeting, The University of Western Australia, 35 Stirling Highway, Crawley 6009, WA, Australia.*

[5]*Géosciences Montpellier, Université Montpellier, UMR-CNRS 5243, Place E. Bataillon, 34090 Montpellier, France.*

[6]*Univ Rennes, CNRS, Géosciences Rennes–UMR 6118, F-35000 Rennes, France.*

[7]*Czech Geological Survey, Prague, Czech Republic.*

Source and deposition age of the Dialé-Daléma metasedimentary series (Kédougou-Kéniéba Inlier, Senegal) constrained by U-Pb geochronology on detrital zircon grains

J. KONE,[1] O. VANDERHAEGHE,[2] F. DIATTA,[3] L. BARATOUX,[2] N. THEBAUD,[4] O. BRUGUIER,[5] P.M. NDIAYE,[3] S. DUCHENE[2] P. PITRA[6,7], J. GANNE,[2]

[1, 2]*IFAN, Cheikh Anta Diop, Dakar, Sénégal.*

[2]*Geosciences Environnement Toulouse, Observatoire Midi Pyrénées, UPS, CNRS, IRD, 14 avenue E. Belin, 31400 Toulouse, France.*

[3]*Département de Géologie, Université Cheikh Anta Diop, Dakar, Sénégal.*

[4]*Centre for Exploration Targeting, The University of Western Australia, 35 Stirling Highway, Crawley 6009, WA, Australia.*

[5]*Géosciences Montpellier, Université Montpellier, UMR-CNRS 5243, Place E. Bataillon, 34090 Montpellier, France.*

[6]*Univ Rennes, CNRS, Géosciences Rennes–UMR 6118, F-35000 Rennes, France.*

[7]*Czech Geological Survey, Prague, Czech Republic.*

Abstract

The Dialé-Daléma metasedimentary series is exposed in the Kédougou-Kéniéba Inlier that corresponds to the northwestern branch of the Eburnean orogenic belt in the southern West African Craton. Here we conducted a U-Pb geochronological study on metapelites, metagraywackes and metavolcanic breccia of the Dialé-Daléma metasedimentary series in order to identify the sedimentary sources and establish the lithostratigraphic sequence of the Kedougou-Kenieba Inlier. This new U-Pb geochronological dataset from five samples representing different stratigraphic levels yield a dominant population of Paleoproterozoic detrital zircon grains with ages ranging from c. 2200 to 2100 Ma. The youngest weighted mean ages at c. 2120 Ma are identical for all five samples within error and provide a maximum deposition age for the sediments of the Dialé-Daléma series. The dominant ages are similar to those obtained on metamorphosed plutonic and volcanic rocks of the Mako belt and thus suggest a dominant proximal source for the clastic sediments of the Dialé-Daléma series and a distal or geographically isolated position relative to the Archean Leo-Man or Réguibat craton nuclei. Deposition ages are only a

few Myr older than available ages for metamorphism and intrusion of plutons forming the Saraya batholith. This is consistent with deposition along an active convergence zone marked by the succession, within a few tens of Myr, of (1) magmatic accretion of the Mako plutonic and volcanic rocks in the context of volcanic arc, associated with local uplift, exhumation and erosion at c. 2200-2160 Ma, (2) deposition of clastic sediments forming the Dialé-Daléma series at c. 2120-2110 Ma followed by (3) their burial and exhumation at c. 2090-2060 partially contemporaneous with (4) the intrusion of the Saraya batholith at c. 2080-2070 Ma.

1 Introduction

U/Pb geochronology on detrital zircon grains from clastic sediments provide important insights into source, timing of sedimentation, stratigraphy and tectonic history that prevailed within convergent and collisional orogenic systems (e.g. Cawood et al., 2012; Grenholm et al., 2019a). The Paleoproterozoic West African Craton exposed in the north-western Africa ‘‘Réguibat rise’’ and the south-western Africa ‘‘Leo-Man rise’’ is extended into the Transamazonian orogenic belt on the other side of the Atlantic (Guyana and Central Brazil Shields) (Abouchami et al., 1990; Boher et al., 1992; Klein and Moura, 2008). These Paleoproterozoic granite-greenstone belts and volcano-sedimentary series that surround the Archaean nuclei, attest to a magmatic-tectonic accretion and reworking by deformation and metamorphism during the Eburnean orogeny between 2.25 and 2.07 Ga (Milési et al., 1989; Ledru et al., 1991; Baratoux et al., 2011; de Kock et al., 2011; Block et al., 2015, 2016; Parra-Avila et al., 2017) and the Transamazonian orogeny 2.26-2.05 Ga (Boher et al., 1992; Abouchami et al., 1990; Vanderhaeghe et al., 1998; Klein and Moura, 2008; Delor, et al., 2003; Milési et al., 2003). Recent studies in the southern West African Craton based on geochronological, structural and geochemical data have documented a diachronous character of the Eburnean collisional orogeny, with the main period of magmatism, sedimentation and tectonothermal activity occurring around c. 2160-2100 Ma in eastern sWAC and between c. 2120-2070 Ma in the west (Hirdes et al., 1996; Hirdes and Davis, 2002; Parra-Avila et al., 2017; Grenholm et 2019a, b).

The reconstruction of the Paleoproterozoic (Birimian / Rhyacian) lithostratigraphic succession, comprising dominantly volcanic greenstone belt and a metasedimentary series has fed a long-standing debate (Kesse, 1985a, b; Milesi et al., 1989; Ledru et al., 1991).

The first lithostratigraphic succession for the Birimian formations of the West African Craton was proposed in Ghana with a dominantly sedimentary series overlain by the dominantly volcanic rocks, locally capped by fluvio-deltaic Tarkwaian deposits (Kitson, 1918; Junner, 1940). As an alternative model, Leube et al. (1990) proposed that volcanic and sedimentary rocks are in lateral continuity and were thus deposited quasi-synchronously. In this model, sediments are intercalated with volcaniclastic rocks and are assumed to represent turbidites derived from the volcanic rocks.

In Senegal, the first proposed model of geosynclinal evolution invoked in contrast, a first phase of emplacement of volcanic rocks followed by deposition of clastic sediments (Bassot, 1963, 1966). This model has been challenged based on structural analysis (Milési et al., 1989; Ledru et al., 1991) arguing for a lower Birimian flysch type unit (B_1), forming the Dialé-Daléma and Kofi series, affected by the three main tectono-metamorphic Eburnean phases (D_1 to D_3), capped by an upper volcanic unit (B_2), exposed in the Mako and Falémé belts, in which the fluvio-deltaic deposits are intercalated and affected only by the two last Eburnean tectono-metamorphic phases (D_2-D_3).

Geochronological data added some constraints feeding this debate. Hirdes & Davis, (2002) proposed a maximum deposition age of c. 2165 Ma for the Dialé-Daléma series, but this age was obtained only on 6 single zircon grains from one metagraywacke sample. A maximum deposition age for the neighboring Kofi metasedimentary series was estimated between c. 2115 and 2098 Ma (Milési et al. 1989; Boher et al., 1992; Allibone et al., in press) on the ground of U-Pb dating of detrital zircon grains. More recently published U-Pb ages suggest that the volcanic rocks of the Mako belt are older than the metasediments of the Dialé-Daléma series (Théveniaut et al., 2010). Moreover, the analysis of geophysical data (magnetic and gravimetric) complemented in the field, revealed that the Mako belt, in contrast to the proposition of Ledru et al. (1991), has also recorded the superposition of D_1 to D_3 structures (Diallo et al., 2020).

In this paper, we present new U-Pb data on detrital zircon grains from the Dialé-Daléma metasediments that provide key information regarding the source(s) and timing of deposition of the sediments and allow to reconstruct the lithostratigraphic succession of the Birimian formations. In addition, these new data also offer insights regarding the paleogeographic and tectonic evolution of the western part of the Eburnean orogenic belt.

2 Geological setting

The southern portion of the West African Craton (sWAC) (Fig. 1a) is referred to as the Leo-Man Rise, which comprises the Kénéma-Man Archean nucleus to the west and the Paleoproterozoic Baoulé-Mossi domain to the east (Bessoles, 1977; Rocci, 1965) (Fig. 1a). The Kénéma-Man Archean nucleus includes migmatite gneisses and tonalite-trondhjemite-granodiorite (TTG) suites forming large domes surrounded by greenstone belts intruded by granitic bodies and charnockites (Black et al., 1980; Feybesse and Milési, 1994, Boher et al., 1992; Cahen et al., 1987; Kouamelan et al., 1997; Potrel et al., 1996; Thiéblemont et al., 2001; Auvray et al., 1992). In the Archean domain two orogenic cycles dated at c.

3.3-3.0 Ga (Leonian) and c. 2.9-2.7 Ga (Liberian) are distinguished (Kouamelan et al., 1997, 2014; Rollinson, 2016). Pre-Leonian rocks dated at c. 3.6-3.4 Ga are preserved as relics of crustal segments within the Leonian, Liberian, Eburnean and Pan-African orogenic belts (Bruguier et al., 1994; Potrel et al., 1996; Kouamelan et al., 1997b; Kroner et al., 2001; Thieblemont et al., 2001; Gouedji et al., 2014). This Archean nucleus was locally reworked during the Eburnean tectono-metamorphic event coincident with deposition of the Paleoproterozoic Birimian (Rhyacian) formations (Kouamelan et al., 1997b; Thieblemont et al., 2004; Pitra et al., 2010; Eglinger et al., 2017).

The Paleoproterozoic is considered by some authors to represent a period of significant juvenile crustal growth (Abouchami et al., 1990; Boher et al., 1992, Taylor et al., 1992; Block et al., 2016, Parra-Avila et al., 2017) pointing to a limited contribution of Archean material (Boher, 1991, Parra-Avila et al., 2017). The Birimian formations comprise a succession of N to NE trending elongated dominantly metavolcanic greenstone belts (Mako and Falémé belts) and metavolcano-sedimentary series (Dialé-Daléma and Kofi series) tectonically accreted during the Eburnean Orogeny (e.g., 2200-2040 Ma: Abouchami et al., 1990; Egal et al., 2002; Thiéblemont et al., 2004; Davis et al., 2015, Masurel et al., 2017). The metavolcanic greenstone belts consist of tholeiitic metabasalts associated with mafic intrusive rocks intercalated with minor immature metasediments, metavolcanics and calcareous rocks. The metavolcano-sedimentary series comprise isoclinally folded and deformed metagreywackes, metapelites and metavolcanic calc-alkaline sequences. Greenstone belts and metavolcano-sedimentary series are intruded by several suites of plutonic rocks, whose geochemical signature ranges from tholeiitic gabbro to high-K calc-alkaline granitoids (Masurel et al., 2016). The oldest crystallization U-Pb ages (2253 ± 9 Ma and 2253 ± 15 Ma) were obtained in the Baoulé-Mossi domain for migmatitic gneisses of dominantly granodioritic composition underlying the Oudalan-Gourouol (Burkina Faso) metavolcano-sedimentary belt (Tshibubudze et al., 2013). Four major pulses of magmatic emplacement have been proposed at c. 2210-2190 Ma, c. 2185-2150 Ma, c. 2115-2100 Ma and c. 2090-2070 Ma (Boher et al., 1992; Davis et al.,1994; Hirdes et al., 1992, 1996; Taylor et al., 1992 de Kock et al., 2011, 2012, Block et al., 2016, Parra-Avila et al., 2017; Grenholm et al., 2019). Nevertheless, these age groups overlap within error, suggesting a continuous period of magmatic activity from c. 2210 to c. 2070 Ma (de Kock et al., 2011, 2012; Block et al., 2016; Parra-Avila et al., 2017).

The few geochronological studies on detrital grains from the metavolcano-sedimentary series of southeastern West African Craton, provide deposition ages bracketed between c.2165 and 2125 Ma (de Kock et al., 2011; Lebrun et al., 2016; Grenholm et al., 2019a).

The metavolcano-sedimentary series are intruded by a series of plutons and provide minimum deposition ages of about 2122-2118 Ma (Maluwé series, de Kock et al., 2011, Block et al., 2016); 2136

± 2 Ma (Kumasi-Afema series, Adadey et al., 2009) and 2088 ± 2 Ma (Sunyani-Comoé series, Hirdes et al., 1992).

The lithological units and ages recorded in the São Luis Craton in the South America correlate with data from the Paleoproterozoic granite-greenstone belts in the southern West African Craton (Feybesse et al., 2006, Klein et al., 2005). However, some studies highlight an early Paleoproterozoic magmatic rocks source that predate the oldest known magmatic rocks in sWAC reported around c. 2250 Ma (Tshibubudze et al., 2013; Parra-Avila et al., 2017). For example, some tonalites and deformed granites provide U-Pb ages of range between 2446 ± 68 Ma and 2231 ± 14 (Almas-Conceição do Tocantins domain, Fuck et al., 2014; de Sousa et al., 2016). In the Bacajá domain, the oldest Paleoproterozoic rocks consist of a quartz-monzodioritic gneiss dated at 2439 ± 4 Ma and a metaandesite at 2359 ± 2 Ma (U-Pb ages: Macambira et al., 2009). Similar Siderian ages have been reported also from a tonalite intruded into the Jacaré Complex (U-Pb ages: 2313 ± 9 Ma, Faraco et al., 2005) and a metatonalite intruded Três Palmeiras greenstone belt (U-Pb ages: 2338 ± 5 Ma, Vasquez et al., 2008). Subsequent plutonic rocks, precisely in French Guiana display petrological and geochemical features pointing to calc-alkaline, peraluminous and metaluminous magmatic series dated at about 2.18-2.13 Ga, 2.11-2.08 Ga, and 2.07-2.06 Ga (Vanderhaeghe et al., 1998; Delor et al., 2003; Milési et al., 2003), respectively.

The Kédougou-Kéniéba Inlier (KKI) (Fig. 1b) represents the westernmost exposure of the Baoulé-Mossi domain in eastern Senegal. In this inlier, Paleoproterozoic formations are characterized by a succession of metavolcanic-plutonic greenstone belts and metavolcanic-metasedimentary series (Junner, 1940), whose lithostratigraphic relationships have been debated (Junner, 1940; Bassot, 1963, 1966, 1987; Milési et al., 1989; Ledru et al., 1991, Feybesse and Milési, 1994, Masurel et al., 2017). On the basis of dominant lithologies character, the KKI is divided into two NE-SW elongated litho-tectonic units (Bassot, 1963, 1966). In the western part of the KKI, the Mako greenstone belt is made of massive and pillowed metabasalts associated with abundant metavolcaniclastics, metatuffs and metacherts. In some places, metabasalt flows are associated with metamorphosed ultrabasic rocks. These metamorphosed ultrabasic to basic rocks have tholeiitic affinities characteristic of MORB (Théveniaut et al., 2010b; Labou et al., 2020). Metaandesitic to rhyolitic rocks of basic to acid composition are also recorded in the Mako belt. The metavolcano-sedimentary rocks include immature metasediments and metavolcanoclastic sediments derived from pyroclastic rocks or erosional products from magmatic edifices. Tholeiitic metabasalt and metaandesite flows from the Mako metavolcanic sequence yield Sm-Nd whole rock isochron ages at 2197 ± 13 Ma and 2160 ± 16 Ma, respectively (Boher et al., 1992, Dia, 1998). The metavolcanic rocks in the Mako belt, exposed in the western part of the KKI, grade to the east to prominent metavolcanoclastic and metasedimentary rocks.

Three main series of plutonic rocks have been identified in the Mako belt based on petrology and geochronology. The first one corresponds to the Badon-Kakadian batholith and Sandikounda amphibolite-gneiss complex dated at c. 2213-2194 Ma (Dia et al., 1997; Hirdes and Davis 2002, Dioh et al., 2006; Gueye et al., 2007). The Sandikounda amphibolite-gneiss complex may represent the deep root of the Mako belt (Dia et al., 1997). The Sandikounda amphibolite-gneiss complex can be interpreted as orthogneiss resulting from the deformation of plutonic rocks forming the Badon-Kakadian batholith or as migmatites resulting from the partial melting of the metavolcano-sedimentary rocks of the Mako belt. The second series corresponds to the Laminia Kaourou plutonic-complex made of granodiorite, tonalite and granite with a calc-alkaline signature and dated between 2138 ± 6 Ma and 2127 ± 6 Ma (Dia et al., 1997). The third series consists of small circular to elliptic shape plutons made of metaluminous hornblende-biotite granodiorite comprising the Tinkoto pluton dated at 2083 ± 6 Ma (Gueye et al., 2007) and the Mamakono pluton dated at 2073 ± 3 Ma (Hirdes and Davis, 2002).

The Dialé-Daléma series, separated from the Mako belt by a high strain zone known as the Main Transcurrent Zone (MTZ), is dominated by metasedimentary rocks comprising metagraywackes, metapelites and metacarbonaceous rocks with interbedded lapilli-metatuffs (Bassot, 1987; Hirdes and Davis, 2002). These metasedimentary rocks are intruded by the Saraya batholith made of several plutonic bodies with a composition ranging from granodiorite to granite (Pons et al., 1992, Delor et al., 2010). Bassot (1963, 1966) first proposed that the Dialé-Daléma series was deposited above the Mako belt in a geosynclinal. Following these authors (Bassot, 1987; Ngom, 1995), the transition between these two units is marked by a metaconglomerate level containing elements of the Mako belt and associated with metandesites, suggesting that the metavolcaniclastic component of Dialé-Daléma metasedimentary series corresponds to a lateral equivalent of the Mako belt (Milési et al., 1989). Previous dating of detrital zircon grains from the metasedimentary series of the Dialé-Daléma yielded ages ranging from 2165 ± 1 Ma to 2117 ± 9 Ma (Hirdes and Davis, 2002, Milési et al., 1989).

The Saraya batholith is made of granitoids ranging from granodiorite to leucogranite associated with a network of pegmatites that were emplaced between 2075 ± 10 Ma and 2072 ± 10 Ma (Delor et al., 2010). Previous ages were obtained on a foliated NE-SW trending muscovite-biotite granite sample containing metamorphic monazites, suggesting a crystallization age at 2079 ± 2 Ma and a metamorphic overprint at 2064 ± 4 Ma (Hirdes and Davis, 2002).

Calc-alkaline volcanic-plutonic rocks, referred to as the Falémé metavolcanic belt, crop out east of the Dialé-Daléma series (Hirdes and Davis 2002, Lawrence et al 2013, Lambert-Smith et al., 2016, Masurel et al., 2017) and are considered as corresponding to a paleogeographic domain different from the Dialé-Daléma series. The geology of the Falémé metavolcanic belt consists of syntectonic granitoids such as

Balangouma and Boboti pluton (Ndiaye et al., 1997, Hirdes and Davis, 2002) dated at 2112 ± 13 Ma and 2089 ± 9 Ma, respectively (Lambert-Smith et al., 2016). Inherited zircons in the Boboti pluton indicate that the early magmatic activity in the Falémé belt occurred at 2218 ± 83 Ma synchronous with the oldest dated units in the Mako belt to the west. Metavolcanic sequences include minor metabasalts, meta-andesite, subordinate metarhyodacite lavas and metapyroclastic rocks interbedded with metavolcaniclastic rocks, metagraywackes and metacarbonate rocks (Hirdes and Davis, 2002).

The eastern part of the KKI, in Mali, is made of the Kofi metasedimentary series which comprises metagraywackes, metapelites and metacarbonate directly east of the Falémé metavolcanic belt (Ledru et al., 1991, Masurel et al., 2017). Almost all geochronological studies have been restricted to the western domain (Dia et al., 1997; Gueye et al., 2007, 2008; Hirdes and Davis, 2002; Delor et al., 2010) and the southeastern domain of the KKI (Hirdes and Davis, 2002; Lambert-Smith et al., 2016; Allibone et al., in press). The timing of granitoid emplacement from Yatela and Sadiola in the Kofi series is constrained in Masurel et al. (2017c). Theses latter rocks show a temporal evolution from c. 2140 - 2080 Ma calc-alkaline metaluminous plutons (e.g., diorite, hornblende-biotite granodiorite) to c. 2080 - 2060 Ma high-K calc-alkaline, metaluminous to slightly peraluminous granites (e.g., biotite-monzogranites) (Masurel et al., 2017). The deposition age of the metasedimentary series has been dated at 2125 ± 27 Ma and 2098 ± 11 Ma, respectively (Boher et al., 1992).

3 Materials and methods

Five samples were selected to represent the Dialé-Daléma metasedimentary series of the KKI (Fig. 2). One sample (J022 ;13.12338, -11.95667) is a metavolcanic breccia selected along the MTZ close to the eastern boundary of the Mako greenstone belt. Another one, (J063 ;13.33260, -11.77226), is a feldspar-rich low-grade metagraywacke, also collected close to the eastern boundary of the Mako greenstone belt but to the southwest of sample J022. Sample MKNT317 (12.62372, -12.24305) was sampled in a riverbed in Kedougou town and consists of a fine to medium grain metasandstone metamorphosed in the greenschist facies. Samples 44a2 (13.19388, -11.54877) and (BKK44 (13.18615499, -11.53743981) are high-grade garnet-bearing metapelite and metagraywacke, respectively, located at the northeastern end of the Saraya batholith. Zircons from samples J022, J063, 44a2 were analyzed at Geosciences Montpellier, Université de Montpellier, whereas samples MKNT317 and BKK44 were analyzed at the Macquarie University.

The samples were crushed and the zircons separated using heavy liquid and Frantz magnetic separator at Géosciences Environnement Toulouse (GET). Statically representative zircons of different morphologies, sizes and colors were then hand-picked from mineral concentrates, mounted and polished for LA-ICPMS analysis. Scanning Electron Microprobe imaging in backscattered electron mode (BSE) was conducted at GET for samples J022, J063, 44a2; and at the Macquarie University for BKK44 and MKNT317.

Samples J022, J063, 44a2 were analyzed by LA-ICP-MS at Geosciences Montpellier. The laser system consists of a Lambda Physik Compex 102 excimer laser coupled to a Thermofinnigan Element XR ICP-MS (AETE-ISO regional facility of the OSU OREME, University of Montpellier). The instrument was tuned for maximum sensitivity and low oxide production (ThO/Th < 1%). Analytical conditions are identical to those reported in previous studies (e.g. Bosch et al., 2011; Bruguier et al., 2017) where ablation experiments were performed under helium, which enhances sensitivity and reduces inter-element fractionation (Gunther and Heinrich, 1999). The helium stream and particles ablated from the sample were mixed with Ar before entering the plasma. Laser spot size was 15 μm for zircons and the laser was operated at a repetition rate of 4Hz using a 12J/cm2 energy density. Total analysis time was 60 s with the first 15 s used for background measurement which was substracted from the sample signal. Before each analysis the surface of the targeted zone was cleaned with 10 pulses using a spot size larger than the size used for U-Pb analysis. Data were acquired in the peak jumping mode using three points per peaks measuring the ^{202}Hg, ^{204}(Pb + Hg), ^{206}Pb, ^{207}Pb, ^{208}Pb and ^{238}U isotopes similarly to the procedure described in Bruguier et al. (2001). Pb/U and Pb/Pb ratios were calibrated against the 91500 crystal (Wiedenbeck et al., 1995). This reference material was analyzed 4 times each five unknowns and was used to correct the measured ratios for mass discrimination (Pb/Pb ratios) and inter-element fractionation (U/Pb ratios). The zircon standard GJ-1 (Jackson et al., 2004) was used as a secondary standard and analysed as an unknown. U-Th-Pb isotopic data were reduced using the Glitter software (van Achterberg et al., 2001) and ages were calculated using Isoplot (Ludwig 2003) and are quoted in the text at the 2σ confidence level.

Samples MKNT317 and BKK44 were analyzed using LA-ICPMS at the CCFS/GEOMOC facilities of Macquarie University. The instrument setup used a Photon Machines Excimer Laser (He1Ex) and an Agilent Technologies 7700 series quadrupole ICP-MS. Analyses were performed using a laser spot size of 40 μm, laser energy set at 100%, 5 Hz repetition rate, an energy setpoint of 4.5, and fluency of 7.59 J/cm2. Each analysis consisted of an initial laser blast to clear the area around the chosen spot, followed by a 60 s period of background reading and a 120 s period of acquisition, during which the ICP-MS was set to measure ^{204}Pb, ^{206}Pb, ^{207}Pb, ^{232}Th, and ^{238}U. ^{235}U is calculated assuming a constant ^{238}U/^{235}U ratio of 137.88. During analysis, the zircon standard GJ-1 (Jackson et al., 2004) was used as the calibrating standard to monitor and correct for instrumental drift. Zircon standards OG-1 (Stern et al.,

2009) and 91500 (Wiedenbeck et al., 1995) were used as secondary standards and analyzed as unknowns. All standards were supplied by the CCFS/GEOMOC facility on a separate mount.

Unknowns were analyzed in runs of 10–15 spots (including spots on each secondary standard), and each run was bracketed by double analyses of the calibrating standard GJ-1. The software GLITTER (Griffin et al., 2008) was used to monitor the quality of the data obtained during the course of analysis. Each run was only initiated after concordant analyses had been obtained from each secondary standard, where on-the-fly processing and plotting of data to determine concordance was made using GLITTER.

The raw data obtained from the LA-ICPMS analyses were reduced using the software Iolite and the U-Pb reduction scheme "U_Pb_geochronology3", which allows for down-hole fractionation correction (Paton et al., 2010, 2011). During data reduction, integrations were made on stable segments of the U, Th and Pb signals obtained during acquisition, and these where subsequently used to calculate ratios and concentrations for each analysis. A smooth spline function was fitted to the GJ-1 standards and used to correct for instrumental drift and calculate the final 2σ propagated error, which is used in all plots presented in this paper. Discordancy for each analysis was calculated using the formulas % disc.=(1−((^{206}Pb/^{238}U age)/ (^{207}Pb/^{206}Pb age)))*100 and % disc.=(1−((^{206}Pb/^{238}U age)/ (^{207}Pb/^{235}U age))) * 100, and only those analyses that were found to be < 5% discordant in both measures were used in age calculations.

The reduced data were subsequently analyzed and plotted using the ISOPLOT 3.75 (Ludwig, 2003) add-in for Microsoft Excel 2003. Determination of age populations within each sample was made using the "unmixing" function in ISOPLOT, which was applied on ^{207}Pb/^{206}Pb ages of concordant spots to constrain subpopulations within the total detrital population.

Accurate common lead correction in zircon during LA-ICP-MS analyses is difficult to achieve, mainly because of the isobaric interference of ^{204}Hg on ^{204}Pb. The contribution of ^{204}Hg on ^{204}Pb was estimated by measuring the ^{202}Hg and assuming a ^{204}Hg/^{202}Hg natural isotopic composition of 0.2298. This allows to monitor the common lead content of the analysed grains, but corrections often result in inaccurate corrected values. Analyses yielding ^{204}Pb close to, or above the limit of detection were then rejected. Table 1 thus presents only analyses for which ^{204}Pb was below detection limit (i.e. no common lead detected). In addition, to make sure that common Pb does not constitute a bias, only concordant analyses were considered in order to establish sediment provenance. Indeed, common Pb can significantly shift the data points on the right of the Concordia diagram, thus biasing the ages to older values. In this study, we used the ^{207}Pb/^{206}Pb ratio as the best age estimate and a discordance threshold of ±5% was considered as a maximum acceptable value. Grains displaying a discordance level higher than ±5% were rejected from the density probability plots and not considered in the discussion.

4 Results

4.1 Sample J022 (metavolcanic breccia)

This sample, collected along the eastern boundary of the Mako greenstone belt, is a metavolcanic breccia interstratified within the Dialé-Daléma metasedimentary series displaying centimeter thick dark grey and brown sedimentary clasts of quarzitic (chert) and carbonate nature (Fig. 2c). Subangular dark clasts of mafic rocks can also be found in the groundmass. The matrix mineralogy is predominantly of intermediate to felsic composition. The metavolcanic breccia unit is foliated and displays a NE trending, NW dipping planar fabric (N035/80NW). This deformation is indicated by preferential alignment of clasts and quartz-chlorite grain in the matrix.

The zircons separated from this sample are strongly fractured rounded fragments. These features are typical of detrital grains. Oscillatory zoning points to a magmatic origin for the initial grains and delineates a tabular and small initial aspect ratio (Fig. 3-J022a to 3-J022d). Some grains contain cavities and inclusions of minerals such as apatite and quartz.

A total of one hundred and twenty analyses were obtained from one hundred-twenty zircons grains that are summarized in table 1 and plotted in Fig. 4a. Thirty-five analyses are strongly discordant, likely due to the fractured state of some of the analyzed grains, and they were rejected in the age calculation. A few isolated $^{207}Pb/^{206}Pb$ ages are defined by single zircon analyses at 2257 ± 15 Ma and 2236 ± 19 Ma. The remaining analyses delineate age peaks at 2174 ± 4 Ma (MSWD = 1.1) for 64 analyses and at 2124 ± 7, (MSWD = 0.5) for 19 analyses (Fig. 4b).

4.2 Sample J063 (low grade metagraywackes)

The outcrop of sample J063 consists of an alternation of muscovite-chlorite schist layers of pelitic nature and feldspar-greywacke sandstone layers with variable grain size displaying abundant small quartz and feldspar clasts. The schist is folded with an axial planar S_n schistosity oriented N30/85NW and a strain slip cleavage (S_{n+1}) that delimits folded microlithons.

Zircon grains separated from this sample are heavily fractured, slightly colorless to light brown. Some of the zircon grains exhibit rounded external shape (Fig. 3-J063j), which is consistent with detrital grains. They display oscillatory zoning, which suggests a magmatic origin (Fig. 3-J063a, 3-J063h, 3-J063k). Most of the zircon grains exhibit tabular-rectangular (Fig. 3-J063b, 3-J063g) and elongated prismatic shape up to 100 µm long with concentric zoning consistent with crystallization in a magma. Some of these grains contain inclusions of apatite and quartz.

One hundred and seven spots have been obtained from one hundred-seven zircon grains from this sample. Results are presented in Table 1 and shown in the concordia diagram and analyses range from concordant to highly discordant (Fig. 4c). Fifty analyses > 5% discordant were rejected in the age calculation (Fig. 4c). A few analyses yield isolated $^{207}Pb/^{206}Pb$ ages ranging from 2288 ± 16 Ma to 2258 ± 16 Ma. The remaining analyses define five age populations at 2229 ± 11 Ma (MSWD = 0.36, n = 6), 2196 ± 8 Ma (MSWD = 0.21, n = 12), 2170 ± 7 Ma (MSWD = 0.22, n = 17), 2148 ± 8 Ma (MSWD = 0.1, n = 14), and 2125 ± 10 Ma (MSWD = 0.21, n = 6).

4.3 Sample MKNT317 (metasandstone)

The dated unit consists of a fine to medium grained sandstone metamorphosed in green schist facies. The sandstone is foliated and displays a north trending, steeply west dipping schistosity (N00/85W).

There are two dominant morphological types of zircons in this sample based on the Pupin's (1980) morphological classification. One type of zircons consists of elongated prism (100) > (110) and well-developed pyramids (211)> (101). In contrast the other type of zircons shows well-developed (101) pyramids and, for some, a rectangular, tabular morphology (Fig. 3-MKNT317a).

Data were collected from seventy-eight zircon grains that are summarized in table 1 and plotted in Fig. 4e. Twenty-one spots > 5% discordant were rejected in the age calculation. A few analyses yield an Archean $^{207}Pb/^{206}Pb$ age of 2691 ± 6 Ma and two isolated Paleoproterozoic ages from 2240 ± 11 Ma and 2209 ± 14 Ma (Fig. 4f). The remaining fifty analyses define two groups based on their $^{207}Pb/^{206}Pb$ ratios. The first group consists of 35 analyses returning a weighted mean age of 2158 ± 4 Ma (MSWD =1.6) (Fig. 4f) and the second group consists of 15 analyses on 15 zircons returning a weighted mean age of 2118 ± 4 Ma (MSWD =2.1).

4.4 Sample 44a2 (garnet-staurolite metapelite)

Sample 44a2 is a garnet-staurolite metapelite collected in the Saraya batholith metamorphic aureole displaying a shallow dipping penetrative metamorphic foliation. The sampled metapelite consists of large porphyroblasts of garnets of radius up to 2mm and of staurolite overgrown by small crystals of garnet in the matrix that contains plagioclase, biotite, white micas and quartz. The metamorphic foliation is NE trending and shallow dipping to NW (N45/10NW).

Zircons isolated from this sample are colorless to pale brown and exhibit an elongated prismatic shape of variable size ranging from 80 to 150 µm long. They display a core-rim texture. Cores are oscillatory zoned suggesting a magmatic origin (Fig. 3-44a2a to 3-44a2b). The oscillatory zoning pattern is overprinted by a porous zone full of inclusions that is interpreted as reflecting in situ dissolution-precipitation (Martin et al., 2006, 2008). A total of twenty analyses have been carried on fifteen zircon grains for U-Pb dating focusing on the cores. The analyses range from concordant to discordant and eleven analyses were rejected on the basis of high discordance or morphological defects (fractures and cavities) (Fig. 5a). Nine concordant to slightly discordant analyses define four age groups based on their $^{207}Pb/^{206}Pb$ ages with a weighted mean age of 2254 ± 17 Ma for 2 analyses, 2227 ± 12 Ma for a single zircon analysis, 2139 ± 16 Ma (MSWD=0.1) for 2 analyses, and 2117 ± 14 Ma (MSWD=0.1) for 4 analyses (Figs. 5a, 5b).

4.5 Sample BKK44 (garnet-staurolite metagraywacke)

Sample BKK44 was also sampled within the Saraya batholith metamorphic aureole. BKK44 is a garnet and staurolite bearing micaschist with a penetrative subhorizontal metamorphic foliation that surround the northern end of Saraya batholith. The rock sample is largely quarzitic in composition with plagioclase, biotite, muscovite, staurolite and garnet. The metamorphic foliation dips shallowly to NW (N35/05NW).

The zircons isolated from this sample are colorless to light brown, and mainly subhedral to euhedral (Fig. 5c, 5d). The crystals are up to 150 μm long, and equant to prismatic. They present a core-rim texture. Cores present concentric oscillatory zoning, typical of crystallization in melt. Low luminescent porous rims full of inclusions overgrowing the cores are interpreted as reflecting in situ dissolution-precipitation (Martin et al., 2006, 2008). A total of thirty-one analyses were obtained from thirty-one zircon grains that are summarized in table 1 and plotted in concordia diagram (Fig. 5e). Twenty spots provide > 5 % discordant $^{207}Pb/^{206}Pb$ ages were rejected in the age calculation. Two of the concordant spots gave single ages of 2237 ± 9 Ma and 2164 ± 9 Ma. The remaining analyses define three age groups based on their $^{207}Pb/^{206}Pb$ ratios at 2149 ± 5 Ma (MSWD= 0.14) for 2 analyses, 2136 ± 13 Ma (MSWD= 2.5) for 3 analyses, and at 2114 ± 11 Ma (MSWD= 2.6) for 4 analyses.

5 Discussion

5.1 Source and deposition age

An assessment of the source of the Dialé-Daléma metasedimentary series requires a synthesis of published geochronological data of potential source areas. Zircon grains in this study yield concordant to nearly concordant ages ranging from c. 2809 to 2100 Ma, documenting four distinct contributions.

An Archean source is pointed out by the presence of a minor population of detrital zircon grains (less than 1% in modal proportion) with ages older than c. 2600 Ma, which might be the Leo-Man Shield or the more distant Réguibat Shield. Recent studies from greenstone belt in southern Mali highlighted also the occurrence of scarce detrital zircon grains that yielded older ages ranging from c. 3600 to 2400 Ma, although there is no record of rocks of this age in the area (Parra-Avila et al., 2016). The Archean nucleus displays ages attributed to the Leonian (c. 3200 – 3100 Ma) and the Liberian (c. 2800 - 2700 Ma) orogenic cycles (Boher et al., 1992; Feybesse and Milési, 1994; Kouamelan et al., 1997; Egal et al., 2002; Thiéblemont et al., 2004, Rollinson 2016). In this study, we therefore infer that the Archean zircon populations derived from the erosion of distal Late Archean rocks.

Another subordinate population of detrital zircon is characterized by early Paleoproterozoic (Siderian) U-Pb ages ranging between 2400 and 2300 Ma, as reported by single spot analyses in the sample J063 2288 ± 16 Ma to 2258 ± 16 Ma. Similar ages of 2324 ± 50 Ma, 2350 ± 8 Ma, 2423 ± 3 Ma were reported as scarce older grains in southern Mali (Massigui region; Wane et al., 2018) and from both eastern and western Baoule-Mossi detrital zircon in stream sediments giving peak at c. 2343 Ma (Parra-Avila et al., 2016). Crystallization ages of similar older magmatic rocks have also been reported from Ghana, interpreted as inherited xenocryst core yielding ages ranging at 2360-2320 Ma (de Kock et al., 2011; Block et al., 2016). The provenance of this Siderian detrital zircon population grains remains speculative because there is no record of these older magmatic events in the current available geochronological dataset of the southern West African Craton (Grenholm et al., 2019a, b). Moreover, the magmatic protolith of the Siderian detrital zircon might correspond to those reported in several domains exposed in the South America Amazonian Craton (Grenholm et al., 2019a). In addition, some of the Paleoproterozoic grains provide ages that range between 2255 and 2200 Ma, and have no equivalent in rocks exposed in the KKI. The source of these old detrital zircons remains unclear, but might either correspond to an early Paleoproterozoic protolith completely eroded in the KKI or to rocks exposed in the eastern part of the Baoulé-Mossi domain. Similar ages of 2253 ± 9 Ma; 2253 ± 15 Ma and 2255 ± 26 Ma have been obtained by Thsibubudze et al. (2013) on granodiorite gneiss, migmatitic gneiss and granite across the Oudalan Gourouol belt (Burkina Faso).

The dominant $^{207}Pb/^{206}Pb$ ages obtained for all analyzed samples from the Dialé-Daléma series span from c. 2200 to 2100 Ma, which is similar to ages of metamorphic and magmatic rocks of the Mako belt dated between c. 2200 and 2070 Ma (Gueye et al., 2008; Hirdes et Davis, 2002; Dia et al 1997, Lambert-Smith et al., 2016). Based on this similarity and on the magmatic texture of the analyzed zircon grains, we argue that the Mako belt represents the major source for the detritus accumulated in the Dialé-Daléma series.

The maximum depositional ages defined by the youngest zircon populations dated in this study range from 2125 ± 10 Ma to 2114 ± 11 Ma. Note that this maximum deposition age is significantly younger than the previously published age of 2165 ± 1 Ma obtained on only six spot analyses (Hirdes and Davis, 2002). The Mako plutonic and volcanic rocks emplaced in the context of volcanic arc must have been locally uplifted and eroded in order to provide the main sedimentary input to the Dialé-Daléma basin. This early volcanic arc stage was followed by tectonic accretion of both the Mako belt and Dialé-Daléma series during the Eburnean orogeny.

5.2 The KKI lithostratigraphy in the West African Craton context

Geochronological data presented in this paper provide new constraints on the lithostratigraphic position of the Dialé-Daléma series relative to the other lithological units of the KKI. Indeed, the identification of detrital zircon grains issued from the Mako belt indicate that deposition of the metasedimentary series postdated emplacement, of the Mako belt. This result contradicts the proposition of a stratigraphic sequence starting with the Dialé-Daléma series overlain by the Mako belt (Kitson, 1928; Junner, 1940; Milési et al., 1989; Ledru et al., 1991) and favors the model of an early emplacement of magmatic rocks of the Mako belt followed by deposition of the sediments, protolith of the Dialé-Daléma series (Bassot, 1963, 1966) or at least in the lateral continuity of the Mako magmatic belt (Leube et al., 1990). On the other hand, the average maximum deposition age ranging from 2125 ± 10 Ma to 2114 ± 11 Ma that we obtained for the metasediments of the Dialé-Daléma series is significantly older than the previously proposed maximum deposition age of c. 2100 Ma for the Kofi metasedimentary series (Milési et al., 1989; Boher et al., 1992) but is similar to the maximum deposition age at 2115 ± 10 Ma recently proposed for the Kofi metasedimentary series from the Loulo district (Allibone et al., in press). It should be noted that Allibone et al. (in press) also describe some zircon grains yielding ages as young as c. 2100 Ma for the Kofi metasediments but they have been interpreted as the product of Pb loss. As such it is unclear whether these ages have a real significance for the age of deposition.

This maximum deposition age of the Dialé-Daléma series is comparable to the deposition age of the Siguiri sedimentary formations exposed in south Mali estimated at c. 2117 Ma (Lebrun et al., 2016). These findings suggest that the studied sedimentary series of the Dialé-Daléma series were deposited before or at the same time as the Kofi series. Deposition of the sedimentary protolith of the Dialé-Daléma metasedimentary series preceded the intrusion of the Saraya batholith at c. 2075-2072 Ma (Delor et al., 2010).

These data, integrated with newly published geochronological data from the KKI, provide a record of the magmatic and tectonic accretion events in this region. Detrital grains of the Dialé-Daléma series suggest that magmatic accretion probably started in the early Paleoproterozoic at c. 2288 Ma. The similar and closest rocks of this age are currently exposed in the in the São Luis Craton in the South America (Faraco et al., 2005; Vasquez et al., 2008; Macambira et al., 2009; Fuck et al., 2014; de Sousa et al.,

2016) and in the eastern part of the Baoulé-Mossi domain (Tshibubudze et al., 2013, Parra-Avila et al., 2017). The geographical extension and geodynamic context of this event are poorly constrained due to the lack of these rocks in the western part of the Baoulé-Mossi domain.

The demonstration, by our provenance study, of a major contribution of rocks eroded from the Mako belt in the Dialé-Daléma series is consistent with the following succession of events : 1) Magmatic accretion of the Mako plutonic and volcanic rocks in the context of volcanic arc, associated with local uplift, exhumation and erosion at c. 2200-2160 (2) deposition of clastic sediments forming the Dialé-Daléma series at c. 2120-2110 Ma followed by (3) their burial and exhumation at c. 2090-2060 partially contemporaneous with (4) the intrusion of the Saraya batholith at c. 2080-2070 Ma. This corresponds to a time lapse of at most 45 - 50 Myrs between deposition and burial of sediments to the depth of intrusion of the batholith, suggesting development of the Dialé-Daléma basin along an active convergence zone.

To the east of the Dialé-Daléma series, magmatism of the Falémé volcanic belt occurred between c.2112 and 2088 Ma (Hirdes and Davis, 2002; Lambert-Smith et al., 2016). According to Lambert-Smith et al. (2016), the volcanic and plutonic rocks in the Falémé Volcanic Belt dominated by dioritic to granodioritic in composition display calc-alkaline metaluminous signatures. Subsequently felsic, peraluminous granite plutons and dykes intruded both Falémé Belt and Koffi series. These results indicate a magmatic differentiation that led to generation of peraluminous, granitic melts with a significant crustal component in the Dialé-Daléma series, the Falémé Volcanic Belt and the Koffi series (Lambert-Smith et al., 2016; Masurel et al., 2017). The deposition age at c. 2115 Ma proposed by Allibone et al. (in press) for the Kofi series is comparable to our ages obtained in the Dialé-Daléma series. When integrated published data, the plutonic rocks including the Boboti and the Balangouma plutons were emplaced between pre-existing series of Dialé-Daléma and Koffi series between 2112 ± 13 Ma and 2088 ± 8 Ma, coincident with felsic volcanism at 2099 ± 4 Ma (Hirdes and Davis, 2002). In turn, the younger deposition age proposed by Boher et al. (1992), would suggest an eastward migration of deposition first of the Dialé-Daléma series followed by the Kofi series.

We suggest that the KKI has recorded a succession of magmatic accretion (Mako belt), followed by deposition of sediments (Dialé-Daléma and Kofi series) in basins that are then progressively tectonically accreted and exhumed during the Eburnean orogeny. This succession might be consistent with a succession of magmatic-tectonic accretion along an active zone of convergence accommodated by a subduction towards the west.

6 Conclusion

A few zircon grains from the Dialé-Daléma series yield Archean and Early Paleoproterozoic (> 2220 Ma) ages, which are unknown in the KKI, suggesting a more distal source that might correspond to rocks currently exposed in the São Luis Craton in the South America, in the southwestern Baoulé-Mossi domain, or in the eastern Baoulé-Mossi domain in Burkina Faso. Most analyzed detrital zircon grains yield ages similar to those of volcanic and plutonic rocks from the Mako belt exposed in the northwestern part of the KKI. This indicates that the Mako belt likely represents the main source for the sediments of the Dialé-Daléma series. In addition, these data show age peaks that range from 2125 ± 10 Ma in the west to ca 2114 ± 11 Ma in the east. These ages constrain the maximum deposition age of the Dialé-Daléma series and indicate that the protoliths of the Dialé-Daléma series are younger than the Mako belt. The magmatic accretion of the Mako belt (c. 2200–2160 Ma) followed by the tectonic juxtaposition of the Mako belt and Dialé-Daléma series and the difference between the youngest detrital zircons of the Dialé-Daléma series (c. 2100 Ma) and the age of the Saraya batholith between (c. 2075 and 2072 Ma) indicates successive magmatic accretion of volcanic and plutonic rocks forming the Mako belt followed by deposition of sediments derived from this belt in a basin that was then tectonically accreted to form the Dialé-Daléma series. These data indicate that the terranes forming the KKI have recorded magmatic and tectonic accretion along an active convergence zone during the Eburnean orogeny.

Acknowledgements

We wish to gratefully acknowledge AMIRA International and the industry sponsors for their support of the WAXI project (P934B). We are also appreciative of the contribution of the various geological surveys department of mines in West Africa as sponsors in kind of WAXI. We thank also the French Embassy in Senegal for the PhD fellowship to Jacques Kone and Nathalie Roubert from Campus France in Toulouse for organizing visits. We are grateful to the reviewers Evandro Klein and Fernando Corfu for their thoughtful and careful comments on this manuscript.

REFERENCES

Abouchami, W., Boher, M., Michard, A., Albarède, F., 1990. A major 2.1 Ga old event of mafic magmatism in West Africa: an early stage of crustal accretion. Geophys. Res. Lett., 95, pp. 17605–17629.

Adadey, K., Théveniaut, H., Clarke, B., Urien, P., Delor, C., Roig, R.J., Feybesse, J.L., 2009. Geological Map Explanation - Map Sheet 0503B (1:100000). CGS/BRGM/Geoman/GSD. (156 pp).

Allibone, A., Lawrence, D., Scott, J., Fanning, M., Lambert-Smith, J., Stenhouse P., Harbidge, R., Vargas, C., Rose Turnbull, R., Holliday, J., in press. Early Paleoproterozoic gold deposits of the Loulo 1 district, western Mali. SEG Special Publication.

Baratoux, L., Metelka, V., Naba, S., Jessell, M.W., Grégoire, M., Ganne, J., 2011. Juvenile Paleoproterozoic crust evolution during the Eburnean orogeny (2.2–2.0 Ga), western Burkina Faso. Precambrian Res. 191, 18–45.

Bassot, J.P., Dommanget, A., 1986. Mise en évidence d'un accident majeur affectantle Protérozoïque inférieur des confins Sénégalo-Maliens: new data on an impor-tant fault in lower Proterozoic on the borders of Senegal and Mali. C. R. Acad.Sci. Sér. 2 Méc. Phys. Chim. Sci. Uni. Sci. De La Terre 302, 1101–1106.

Bassot, J.P. 1966. Etude géologique du Sénégal oriental et de ses confins Sénégalo-Maliens. Mém B.R.G.M., 40 ;322p

Bassot, J.P., 1987. Le complexe volcano-plutonique calco-alcalin de la rivière Daléma (Est Sénégal) : discussion de sa signification géodynamique dans le cadre de l'orogénie éburnéenne (Protérozoïque inferieur). Journal African Earth Sciences 64, 505–519.

Bessoles, B., 1977. Geologie de l'Afrique : Le craton Ouest-Africain. Memoires du BRGM, vol. 88, 403 p.

Black, R., Bayer, R., Lesquer, A., 1980. Evidence for late Precambrian plate tectonicsin West Africa (reply). Nature 284 (5752), 192-192.

Block, S., Baratoux, L., Zeh, A., Laurent, O., Bruguier, O., Jessell, M., Ailleres, L., Sagna, R., Parra-Avila, L.A., Bosch, D., 2016a. Paleoproterozoic juvenile crust formation and stabilisation in the south-eastern West African Craton (Ghana) ; new insights from UPb-Hf zircon data and geochemistry. Precambrian Res. 287, 1–30.

Block, S., Ganne, J., Baratoux, L., Zeh, A., Parra-Avila, L.A., Jessell, M., Ailleres, L., Siebenaller, L., 2015. Petrological and geochronological constraints on lower crust exhumation during Paleoproterozoic (Eburnean) orogeny, NW Ghana, West African Craton. J. Metamorph. Geol. 33, 463–494.

Boher, M., Abouchami, W., Michard, A., Albarede, F., Arndt, N.T., 1992. Crustal growth in West Africa at 2.1 Ga. J. Geophys. Res.: Solid Earth 97 (B1), 345–369.

Bosch, D., Garrido, C.J., Bruguier, O., Dhuime, B., Bodinier, J.L., Padròn-Navarta, J.A., Galland, B., 2011. Building an island-arc crustal section: Time constraints from a LA-ICP-MS zircon study. Earth Planet. Sci. Lett. 309, 268–279.

Bruguier, O., Dada, S., Lancelot, J.R., 1994. Early Archean component (>3.5 Ga) within a 3.05 Ga orthogneiss from northern Nigeria: U-Pb zircon evidence. Earth Planet. Sci. Lett. 125, 89-103.

Bruguier, O., Telouk, P., Cocherie, A., Fouillac, A.M., Albarede, F., 2001. Evaluation of Pb-Pb and U-Pb laser ablation ICP-MS zircon dating using matrix-matched calibration samples with a frequency quadrupled (266 nm) Nd-YAG laser. Geostandards Newsletter 25, 361-373.

Bruguier, O., Bosch, D., Caby, R.,Vitale-Brovarone, A., Fernadez, L., Hammor, D., Laouar, R., Ouabadi, A., Abdallah, N., Mechati, M. 2017. Age of UHP metamorphism in the western Mediterranean: insights from rutile and minute zircon inclusions in a diamond-bearing garnet megacryst (Edough Massif, NE Algeria). Earth Planet. Sci. Lett. 474, 215–225.

Cawood, P.A., Nemchin, A.A., Freeman, M., Sircombe, K., 2003. Linking source and sedimentary basin: detrital zircon record of sediment flux along a modern river system and implications for provenance studies. Earth Planet Sci. Lett. 210, 259–268.

Cawood, P.A., Hawkesworth, C.J., Dhuime, B., 2012. Detrital zircon record and tectonic setting. Geology 40, 875–878.

Davis, D.W., Hirdes, W., Schaltegger, U., Nunoo, E.A., 1994. U-Pb age constraints on deposition and provenance of Birimian and gold-bearing Tarkwaian sediments in Ghana, West Africa. Precambrian Res. 67, 89–107.

Diallo, M., Lenka, B., Dufréchou, G., Jessel, M.W., Vanderhaeghe, O., Ly, S., Baratoux, D., 2020. Structure of the Paleoproterozoic Kédougou-Kéniéba Inlier (Senegal-Mali) deduced from gravity and aeromagnetic data. J. Afr. Earth Sci. 162 (2020) 103732.

de Kock, G.S., Armstrong, R.A., Siegfried, H.P., Thomas, E., 2011. Geochronology of the Birim supergroup of the West African craton in the Wa-Bolé region of west-central Ghana: Implications for the stratigraphic framework. J. Afr. Earth Sci. 59, 1–40.

de Kock, G.S., Théveniaut, H., Botha, P.M.W., Gyapong, W., 2012. Timing the structural events in the Palaeoproterozoic Bolé-Nangodi belt terrane and adjacent Maluwe basin, West African craton, in central-west Ghana. J. Afr. Earth Sci. 65, 1–24.

Dia, A., 1988. Caractères et signification des complexes magmatiques et métamorphiques du secteur de Sandikounda-Laminia (Nord de la boutonnière de Kédougou, Est du Sénégal) : un modèle géodynamique du Birimien de l'Afrique de l'Ouest. Unpublished Ph.D. Thesis, Université de Dakar, Sénégal, 350p.

Dia, A., Van Schmus, W.R., Kroner, A., 1997. Isotopic constraints on the age and formation of a Palaeoproterozoic volcanic arc complex in the Kedougou Inlier, eastern Senegal, West Africa. J. Afr. Earth Sci. 24, 197–213.

Delor, C., Lahondère, D., Egal, E., Lafon, J.M., Cocherie, A., Guerrot, C. & de Avelar, V., 2003. Transamazonian crustal growth and reworking as revealed by the 1:500,000-scale geological map of French Guiana. Géologie de la France 2003 2-3-4: 5–57.

Delor, C., Couëffé, R., Goujou, J.C., Diallo, D.P., Théveniaut, H., Fullgraf, T., Ndiaye, P.M.,Dioh, E., Blein, O., Barry, T.M.M., Le Métour, J., Martelet, G., Sergeev, S., Wemmer,K., 2010. Notice explicative de la carte géologique à 1/200 000 du Sénégal, feuilleSaraya-Kédougou Est. Ministère des Mines, de l'Industrie, de l'Agro-Industrie etdes PME, Direction des Mines et de la Géologie, Dakar.

de souse, I.S.M., Giustina, M.E.S.D., Oliveira, C.G., 2019. Crustal evolution of the northern Brasília Belt basement, centralBrazil: A Rhyacian orogeny coeval with a pre-Rodinia supercontinentassembly. Precambrian Research 273 (2016) 129–150.

Dioh, E., Béziat, D., Debat, P., Grégoire, M., Ngom, P.M., 2006. Diversity of the Paleoproterozoic granitoids of the Kédougou inlier (eastern Senegal): petrographical and geochemical constraints. J. Afr. Earth Sci. 44, 351–371.

Egal, E., Thiéblemont, D., Lahondère, D., Guerrot, C., Costea, C.A., Iliescu, D., Delor, C.,Goujou, J.-C., Lafon, J.M., Tegyey, M., Diaby, S., Kolié, P., 2002. Late Eburnean granitization and tectonics along the western and northwestern margin of the Archean Kénéma-Man domain (Guinea, West African Craton). Precambrian Res. 117, 57–84.

Eglinger, A., Thébaud, N., Zeh, A., Davis, J., Miller, J., Parra-Avila, L.A., Loucks, R.,McCuaig, C., Belousova, E., 2017. New insights into the crustal growth of the Paleoproterozoic margin of the Archean Kéména-Man domain, West African craton (Guinea): implications for gold mineral system. Precambrian Res. 292, 258–289.

Faraco, M.T.L, Vale, A.G., Santos, J.O.S., Luzardo, R., Ferreira, A.L., Oliveira, M.A., Marinho, P.A.C., 2005. Levantamento Geologico da Regiao ao Norte da Provıncia Carajas. In: Souza, V.S., Horbe, A.M.C. (Eds.), Contribuicoes a Geologia da Amazon. 4, 32–44.

Feybesse, J.-L., Milési, J.-P., 1994. The Archaean/Proterozoic contact zone in West Africa: a mountain belt of décollement thrusting and folding on a continental margin related to 2.1 Ga convergence of Archaean cratons? Precambrian Res. 69, 199–227.

Feybesse, J.-L., Billa, M., Guerrot, C., Duguey, E., Lescuyer, J.-L., Milesi, J.-P., Bouchot, V., 2006. The paleoproterozoic Ghanian province: geodynamic model and ore controls, including regional stress modelling. Precambrian Res. 149, 149–196.

Fuck, R.A., Dantas, E.L., Pimentel, M.M., Botelho, N.F., Armstrong, R., Laux, J.H.,Junges, S.L., Soares, J.E., Praxedes, I.F., 2014. Paleoproterozoic crust-formationand reworking events in the

Tocantins Province, Central Brazil: a contributionfor Atlantica supercontinent reconstruction. Precambrian Res. 244, 53–74.

Gouedji, F., Picard, C., Coulibaly, Y., Audet, M.-A., Auge, T., Goncalves, P., Paquette, J.-L., Ouattara, N., 2014. The Samapleu mafic–ultramafic intrusion and its Ni–Cu-PGE mineralization: an Eburnean (2.09 Ga) feeder dyke to the Yacouba Layered Complex (Man Archean craton, western Ivory Coast). Bull. Soc. Geol. France 185,393–411.

Günther, D., Heinrich, C.A., 1999. Enhanced sensitivity in LA–ICP–MS using helium–argon mixture as aerosol carrier. J. Anal. At Spectrom.14, 1369–1374.

Griffin, W.L., Powell, W., Pearson, N., O'Reilly, S., 2008. GLITTER: data reduction software for laser ablation ICP-MS, Laser Ablation-ICP-MS in the Earth Sciences. Mineral. Assoc. Can. Short Course Ser. 40, 204–207.

Gueye, M., Siegesmund, S., Wemmer, K., Pawlig, S., Drobe, M., Nolte, N., Layer, P.,2007. New evidence for an early Birimian evolution in the West African Craton: an example from the Kédougou-Kéniéba inlier, southeast Senegal. S. Afr. J. Geol.110, 511–534.

Grenholm, M., Jessel, M., Thébaud, N., 2019a. Paleoproterozoic volcano-sedimentary in the ca. 2.27-1.96 Ga Birimian orogen of the southern West African Craton. Precambrian Research 328 (2019) 161-192.

Grenholm, M., Jessel, M., Thébaud, N., 2019b. A geodynamic model for the Paleoproterozoic (ca. 2.276-1.96 Ga) Birimian Orogen of the southern West African Craton – Insights into an evolving accretionary-collisional orogenic system. Earth-Science Reviews 192 (2019) 138–193.

Hirdes, W., Davis, D.W., Eisenlohr, B.N., 1992. Reassessment of Proterozoic granitoid ages in Ghana on the basis of U/Pb zircon and monazite dating. Precambrian Res.56, 89–96.

Hirdes, W., Davis, D.W., Ludtke, G., Konan, G., 1996. Two generations of Birimian (Paleoproterozoic) volcanic belts in northeastern Cote d'Ivoire (West Africa): consequences for the 'Birimian controversy'. Precambrian Res. 80, 173–191.

Hirdes, W., Davis, D.W., 2002. U-Pb Geochronology of Palaeoproterozoic rocks in the southern part of the Kédougou-Kéniéba inlier, Senegal, West Africa: evidence for diachronous accretionary development of the Eburnean Province. Precambrian Res. 118, 83–99.

Jackson, S.E., Pearson, N.J., Griffin, W.L., Belousova, E.A., 2004. The application of laserablation-inductively coupled plasma-mass spectrometry to in situ U-Pb zircongeochronology. Chem. Geol. 211, 47–69.

Junner, N.R., 1940. Geology of the Gold Coast and Western Togoland. Gold Coast Geol. Surv. Bull. 11 (11), 1–40.

Kesse, G.O., 1985. The Mineral and Rock Resources of Ghana. Kitson, A.E., 1918. Annual Report. Gold Coast Geological Survey for 1916/17, Accra. (non publ.), Accra.

Kitson, A. E., 1918. Annual Report for 1916/17. In: Gold Coast Geological Survey, Accra, Ghana.

Klein, E.L., Moura, C.A.V., Pinheiro, B.L.S., 2005. Paleoproterozoic crustal evolution of the Sao Luís Craton, Brazil: evidence from zircon geochronology and Sm-Nd isotopes. Gondwana Res. 8, 177–186.

Klein, E. L., Moura, C.A.V., 2008. Sao Luis craton and Gurupi Belt (Brazil): possible links with the West African Craton and surrounding Pan-African Belt. Geological Society, London, Special publications: 294. pp. 137-151.

Kouamelan, A.N., Peucat, J.-J., Delor, C., 1997a. Reliques archeennes (3.15 Ga) au sein du magmatisme birimien (2.1 Ga) de Côte d'Ivoire, craton ouest-africain. C. R.l'Academie Sci. Paris 324, 719–727.

Kouamelan, A.N., Delor, C., Peucat, J.-J., 1997b. Geochronological evidence for reworking of Archaean terrains during the Early Proterozoic (2.1 Ga) in the western Cote d'Ivoire (Man Rise – West African Craton). Precambr. Res. 86, 177–199.

Kroner, A., Ekwueme, B.N., Pidgeon, R.T., 2001. The oldest rocks in West Africa: SHRIMP zircon age for Early Archean migmatitic orthogneiss at Kaduna, Northern Nigeria. J. Geol. 109, 399–406.

Labou, I., Benoit, M., Baratoux, L., Grégoire, M., Ndiaye, PM., Béziat, B., Debat, P., Thébaud N., 2019. Petrological and geochemical study of Birimian ultrabasic rocks within the West African Craton: insights from Mako (Senegal) and Loraboué (Burkina Faso) lherzolite/harzburgite/wehrlite associations.

Lambert-Smith, J.S., Lawrence, D.M., Müller, W., Treloar, P.J., 2016. Paleoprotectonic setting of the southeastern Kédougou-Kénieba inlier, West Africa: new insights from igneous trace element geochemistry and U-Pb zircon ages. Precambr. Res. 274, 110–135.

Leube, A., Hirdes, W., Mauer, R., Kesse, G.O., 1990. The early Proterozoic BirimianSupergroup of Ghana and some aspects of its associated gold mineralization.Precambrian Res. 46 (1), 139

Ledru, P., Pons, J., Milesi, J.P., Feybesse, J.L., Johan, V., 1991. Transcurrent tectonics and polycyclic evolution in the Lower proterozoic of Senegal-Mali. Precambr. Res. 50, 337–354.

Ludwig,. K.R.,. 2003. Isoplot/Ex. A geochronological toolkit for Microsoft Excel. Berkeley Geochronological Centre,. Special Publication 4,. 71pp.

Macambira, M.J.B., Vasquez, M.L., Silva, D.C.C., Galarza, M.A., Barros, C.E.M., Camelo, J.F., 2009. Crustal growth of the central eastern Paleoproterozoic domain, SW Amazonian craton: juvenile accretion vs. reworking. J. S. Am. Earth Sci. 27, 235–246.

Martin, L., Duchêne, S., Deloule, E., Vanderhaeghe, O., 2006. The isotopic composition of zircon and garnet: a record of the metamorphic history of Naxos, Greece. Special volume “Geochronology of Metamorphism, Deformation and Metallogenesis”. Lithos 87, 174–192.

Martin, L., Duchêne, S., Deloule, E., Vanderhaeghe, O., 2008. Mobility of trace elements and oxygen isotopes during metamorphism: consequences on geochemical tracing. Earth Planet. Sci. Lett. 267, 161–174.

Milési, J.P., Feybesse, J.L., Ledru, P., Dommanget, A., Ouedrago, M., Marcoux, E., Prost,A., Vinchon, C., Sylvain, J.P., Johan, V., Tegyey, M., Calvez, J.Y., Lagny, P., 1989. West African gold deposits in their Lower Proterozoic lithostructural setting. Chronique de la Recherche Miniere 497, 3–98.

Milesi J.P., Lerouge C., Delor C., Ledru P., Billa M., Cocherie A., Egal E., Fouillac A.M., Lahondere D., Lasserre J.L., Marot A., Martel-Jantin B., Rossi P., Tegyey M., Théveniaut H., Thiéblemont D., Vanderhaeghe O., (2003). Gold deposits (gold-bearing tourmalinites, gold-bearing conglomerates, and mesothermal lodes), markers of geological evolution of French Guiana. Geology, metallogeny and stable-isotope constraints. Géologie de la France, 2, 257-290.

Milesi, J., Feybesse, J.., Pinna, P., Deschamps, Y., Kampunzu, H., Muhongo, S., Lescuyer, J.L., Le Goff, E., Delor, C., Billa, M., Ralay, F., Heinry, C., 2004. Geological map of Africa 1:10000000 SIGAfrique project. In: 20th Conference of African Geology, BRGM, Orleans, France, 2-7 June, http://www.sigafrique.net (lastaccessed 14/12/2010).

Ndiaye, P.M., Dia, A., Vialette, Y., Diallo, D.P., Ngom, P.M., Sylla, M., Wade, S., and Dioh, E., 1997, Données pétrographiques, géochimiques et géochronologiques nouvelles sur les granitoïdes du Paléoprotérozoïque du Supergroupe de Dialé-Daléma (Sénégal Oriental): implications pétrogénétiques et géodynamiques: Journal of African Earth Sciences, v. 25, p. 193–208

Ngom, P.M., 1995. Caractérisation de la croûte Birimienne dans les parties centrale et méridionale du supergroupe de Mako. Implications géochimiques et pétrogénétiques. Thèse de doctorat d'état Univ. Cheikh Anta Diop, Dakar, Sénégal. 240 p.

Paton, C., Woodhead, J.D., Hellstrom, J.C., Hergt, J.M., Greig, A., Maas, R., 2010.Improved laser ablation U-Pb zircon geochronology through robust downholefractionation correction. Geochem. Geophys. Geosyst. 11, Q0AA06, http://dx.doi.org/10.1029/2009GC002618

Paton, C., Hellstrom, J., Paul, B., Woodhead, J. and Hergt, J. 2011. Iolite: freeware for the visualization and processing of mass spectrometer data. Journal of Analytical Atomic Spectrometry 26, 2508-2518.

Parra-Avila, L.A., Kemp, A.I.S., Fiorentini, M.L., Belousova, E., Baratoux, L., Block, S., Jessell, M., Bruguier, O., Begg, G.C., Miller, J., Davis, J., McCuaig, T.C., 2017. The geochronological evolution of the Paleoproterozoic Baoulé-Mossi domain of the southern West African Craton. Precambr. Res. 300, 1–27.

Pitra, P., Kouamelan, A.N., Ballevre, M., Peucat, J.J., 2010. Palaeoproterozoic highpressure granulite overprint of the Archean continental crust: evidence for homogeneous crustal thickening (Man Rise, Ivory Coast). J. Metamorph. Geol. 28, 41–58.

Potrel, A., Peucat, J.J., Fanning, M., Auvray, B., Burg, J.P., Caruba, C., 1996. 3.5 Ga old terranes in the West African Craton, Mauritania. J. Geol. Soc., London 153, 507–510.

Poitrasson F., Chenery S., Shepperd T.J., 2000. Electron microprobe and LA-ICP-MS study of monazite hydrothermal alteration: Implications for U–Th–Pb geochronology and nuclear ceramics. Geochim. Cosmochim. Acta 64, 3283–3297

Pupin, J. P. (1980). Zircon and granite petrology. Contributions to Mineralogy and Petrology 73, 207–220.

Stern, R.A., Bodorkos, S., Kamo, S.L., Hickman, A.H. and Corfu, F. 2009. Measurement of SIMS Instrumental Mass Fractionation of Pb Isotopes During Zircon Dating. Geostandards and Geoanalytical Research, 33, 145-168.

Rollinson, H., 2017, There were no large volumes of felsic continental crust in the early Earth: Geosphere, v 13, no 2, p. 235-246, doi:10.1130/GES01437.1.

Taylor, P.N., Moorbath, S., Leube, A., Hirdes, W., 1992. Early Proterozoic crustal evo-lution in the birimian of Ghana: constraints from geochronology and isotopegeochemistry. Precambrian Res. 56 (1–2), 97–111.

Théveniaut, H., Ndiaye, P.M., Buscail, F., Couëffé, R., Delor, C., Fullgraf, T., Goujou, J.-C., 2010. Notice explicative de la carte géologique du Sénégal oriental à 1/500 000. Ministère des Mines, de l'Industrie, de l'Agro-Industrie et des PME, Direction des Mines et de la Géologie, Dakar.

Thieblemont, D., Delor, C., Cocherie, A., Lafon, J.M., Goujou, J.C., Balde, A., Bah, M., Sane, H., Fanning, C.M., 2001. A 3.5 Ga granite-gneiss basement in Guinea: further evidence for early archaean accretion within the West African Craton. Precambr. Res. 108, 179–194.

Thieblemont, D., Goujou, J.C., Egal, E., Cocherie, A., Delor, C., Lafon, J.M., Fanning, C.M., 2004. Archaean evolution of the Leo Rise and its Eburnean reworking. J. Afr. Earth Sci. 39, 97–104.

Tshibubudze, A., Hein, K.A.A., Peters, L.F.H., Woolfe, A.J., McCuaig, T.C., 2013. Oldest UPb crystallisation age for the West African Craton from the Oudalan-Gorouol Belt of Burkina Faso. S. Afr. J. Geol. 116, 169–181.

Van Achterberg,. E.,. Ryan,. C.G.,. Jackson,. S.E. Griffin,. W.L.,. 2001. Data reduction software for LA-ICP-MS: appendix. In: Sylvester,. P.J. (Ed.),. Laser ablation-ICP- Mass Spectrometry in the Earth Sciences: Principles and Applications. Mineralogical Association of Canada,. Short Course Series,. Ottawa,. Ontario,. Canada 29,. 239-243.

Vanderhaeghe, O., Ledru, P., Thiéblemont, D., Egal, E., Cocherie, A., Tegyey, M., & Milési, J.-P., 1998, Contrasting mechanism of crustal growth. Geodynamic evolution of the Paleoproterozoic granite-greenstone belts of French Guiana: Precambrian Research, v. 92, p. 165-193.

Vasquez, M.L., Macambira, M.J.B., Armstrong, R.A., 2008. Zircon geochronology of granitoids from the western Bacaja domain, southeastern Amazonian craton, Brazil: Neoarchean to Orosirian evolution. Precambrian Res. 161, 279–302.

Wane, O., Liégeois, J.P., Thébaud, N., Miller, J., Metelka, V., Jessell, M., 2018. The onset of the Eburnean collision with the Kenema-Man craton evidenced by plutonic and volcanosedimentary rock record of the Masssigui region, southern Mali. Precambrian Research 305 (2018) 444–478.

Wiedenbeck, M., Alle, P., Corfu, F., Meier, M., Overli, F, Von Quadt, A., Roddick, J.C. and Spiegel, W. 1995. Three natural zircon standards for U-Th-Pb, Lu-Hf, trace element and REE analysis. Geostandards Newsletter, 1-23.

Figure captions

Figure 1. (1a) The southern portion of the West African Craton showing the study area, modified after (Milési et al., 2004). (1b) Litho-structural map of the KKI showing the locations of dated samples (modified after Hirdes & Davis, 2002; Dioh et al., 2006).

Figure 2. (a) MKNT317 fine to medium grained metasandstone sampled in a riverbed close to Kedougou town. (b) Metasandstone sample MKNT317. (c) J022 metavolcanics breccia collected at the Mako and Dialé-Daléma transition zone. (d) J063 outcrop photograph showing folded metagraywacke. (e) Garnet bearing metapelites, sample 44a2 collected in the high-grade metasedimentary rocks at the northern end of the Saraya granite. (f) Outcrop of garnet bearing metagraywackes, sample BKK44 collected in the high-grade metasedimentary rocks at the northern end of the Saraya granite.

Figure 3. Back-scattered electron images of representative zircons for each age population in dated samples (J022, J063, MKNT317, 44a2).

Figure 4. Dialé-Daléma metasedimentary series age distribution in concordia diagrams and probability density diagrams based on $^{207}Pb/^{206}Pb$ ages of concordant analysis. Data in red color are concordant to semi-concordant, whereas data in green color are < 5% discordant spots. (4a) Concordia diagram constructed from 120 spot analyses for sample J022. (4b) Age distribution histograms for concordant to semi-concordant spot analyses from sample J022. (4c) Concordia diagram constructed from 107 spots for sample J063. (4d) Age distribution histograms for concordant to semi-concordant spot analyses from sample J063. (4e) Concordia diagram constructed from 78 spot analyses for sample MKN317. (4f) Age probability density plot showing age distribution for concordant to semi-concordant analyses for MKNT317.

Figure 5. Dialé-Daléma metasedimentary series ages distribution in Concordia diagrams and probability density diagrams based on $^{207}Pb/^{206}Pb$ ages of concordant and semi-concordant spots only. Data in red color are concordant to semi-concordant, whereas data in green color are < 5% discordant spots. (5a) Concordia diagram constructed from 20 analyses for sample 44a2. (5b) Age distribution histogram for 9 concordant to semi-concordant analyses from sample 44a2. (5c, 5d) Scanning Electron Microscopy

(SEM) images of representative zircons for sample BKK44. (5e) Concordia diagram constructed from 31 spots from sample BKK44. (5f) probability density plot for 11 concordant to semi-concordant spots showing the age distribution of detrital zircons from sample BKK44.

Table 1. Summary of U-Pb analytical data for samples J022, J063, MKNT317,44a2 and BKK44.

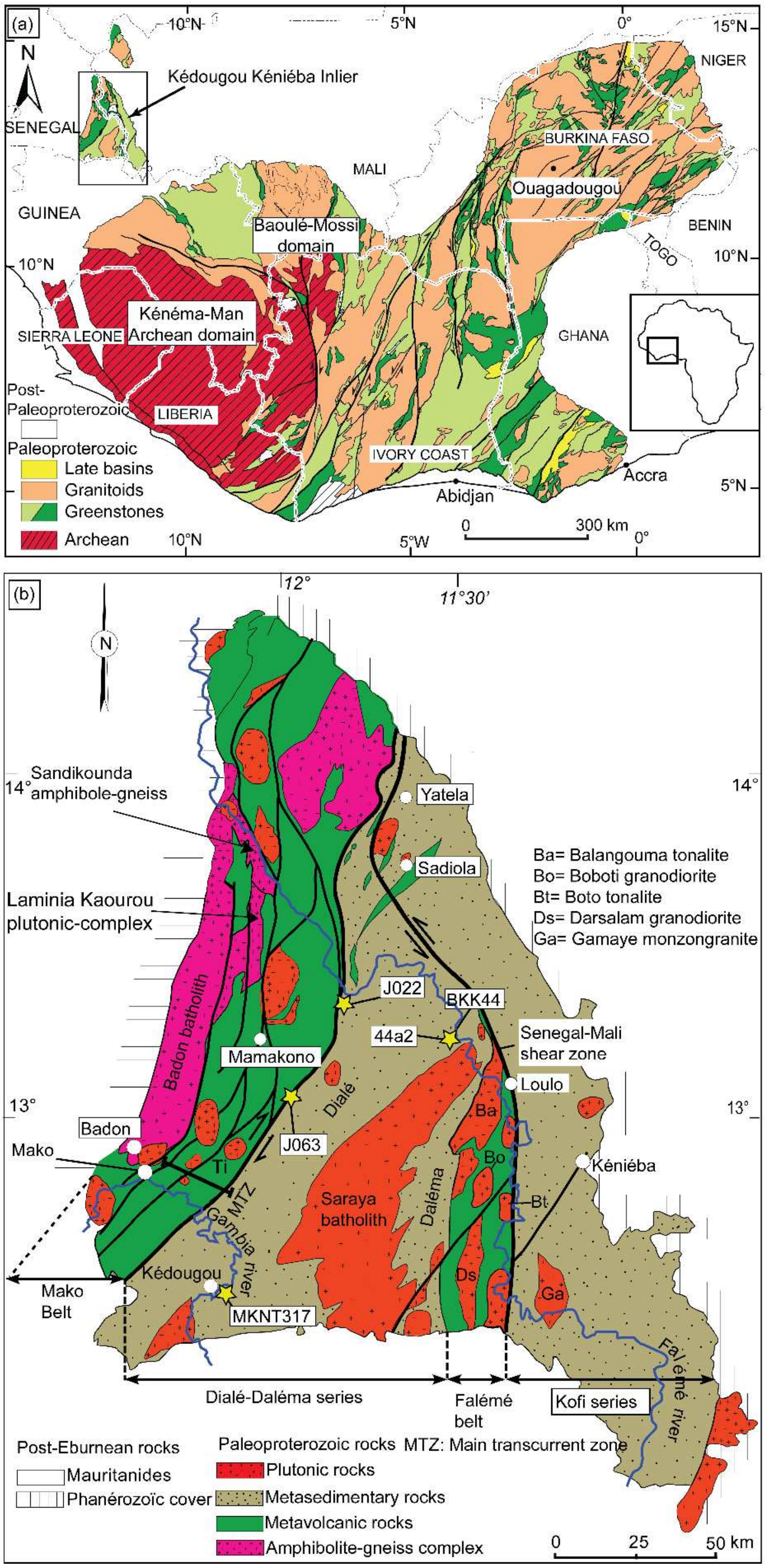

875

876 Figure 1.

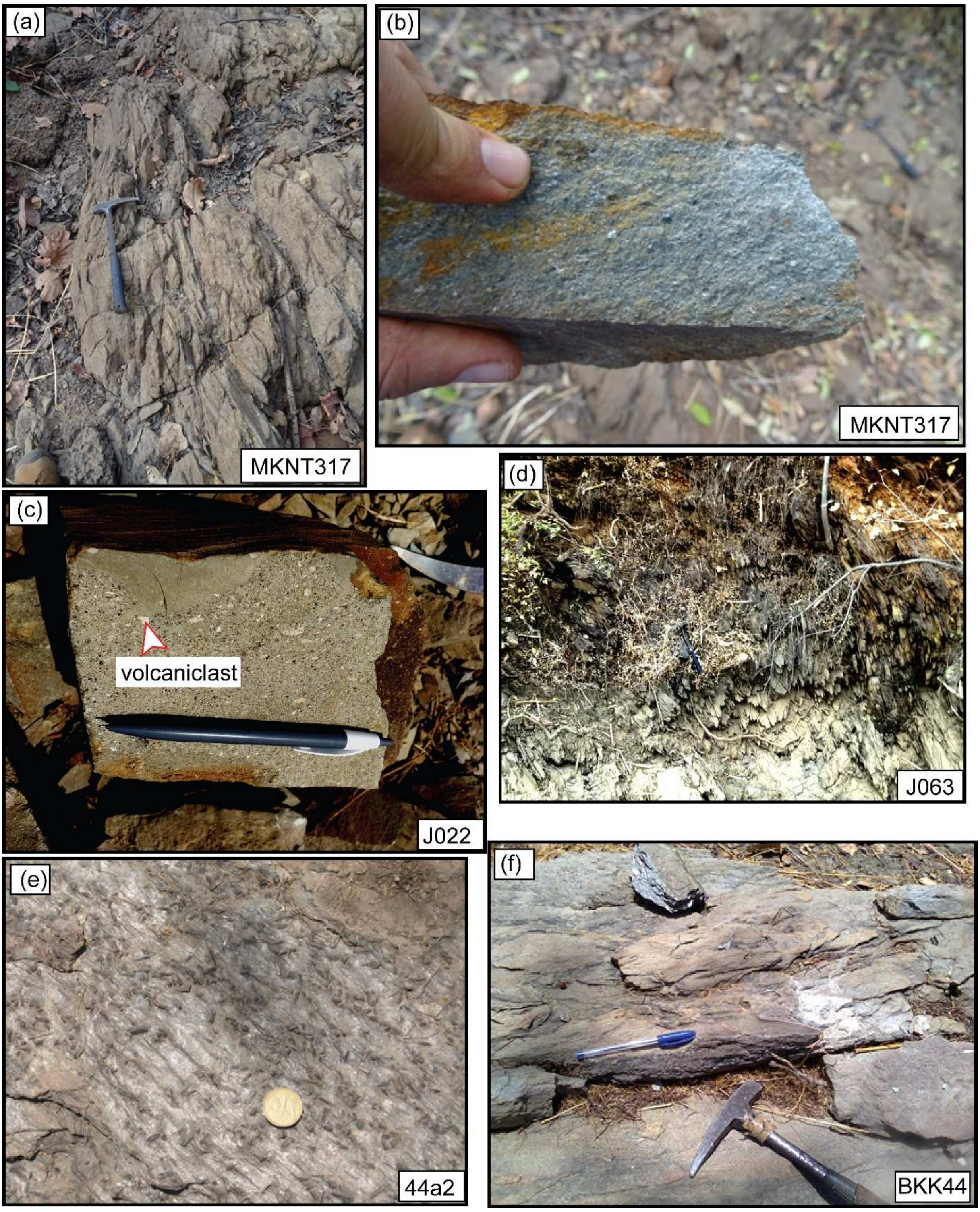

877

878 Figure 2.

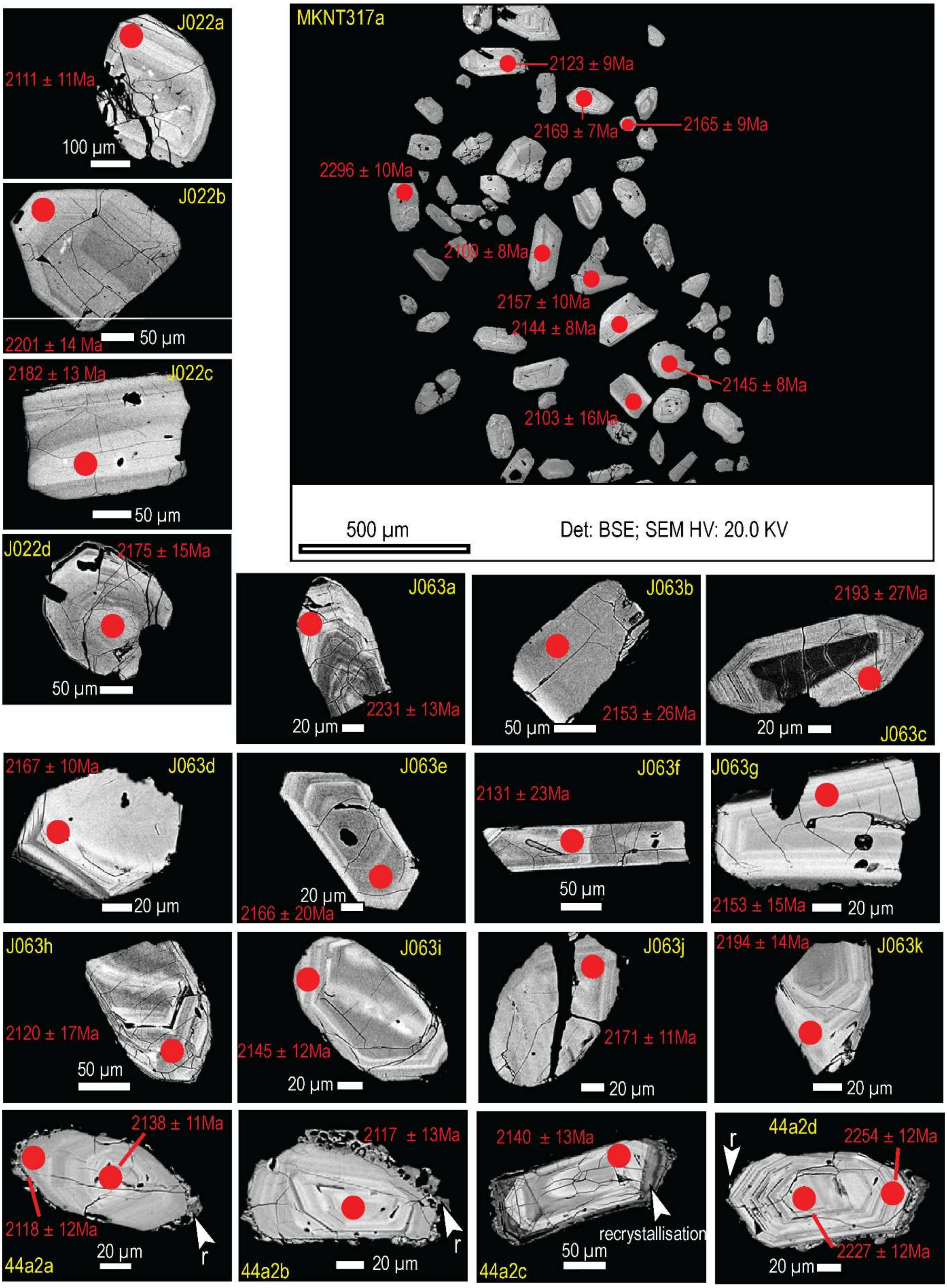
J022a
2111 ± 11Ma
100 µm
J022b
2201 ± 14 Ma
50 µm
2182 ± 13 Ma
J022c
50 µm
J022d
2175 ± 15Ma
50 µm
MKNT317a
2123 ± 9Ma
2169 ± 7Ma
2165 ± 9Ma
2296 ± 10Ma
2109 ± 8Ma
2157 ± 10Ma
2144 ± 8Ma
2145 ± 8Ma
2103 ± 16Ma
500 µm
Det: BSE; SEM HV: 20.0 KV
J063a
2231 ± 13Ma
20 µm
J063b
2153 ± 26Ma
50 µm
2193 ± 27Ma
20 µm
J063c
2167 ± 10Ma
J063d
20 µm
J063e
20 µm
2166 ± 20Ma
J063f
2131 ± 23Ma
50 µm
J063g
2153 ± 15Ma
20 µm
J063h
2120 ± 17Ma
50 µm
J063i
2145 ± 12Ma
20 µm
J063j
2171 ± 11Ma
20 µm
2194 ± 14Ma
J063k
20 µm
2138 ± 11Ma
2118 ± 12Ma
20 µm
r
44a2a
2117 ± 13Ma
r
44a2b
20 µm
2140 ± 13Ma
recrystallisation
50 µm
44a2c
r
44a2d
2254 ± 12Ma
2227 ± 12Ma
20 µm

Figure 3.

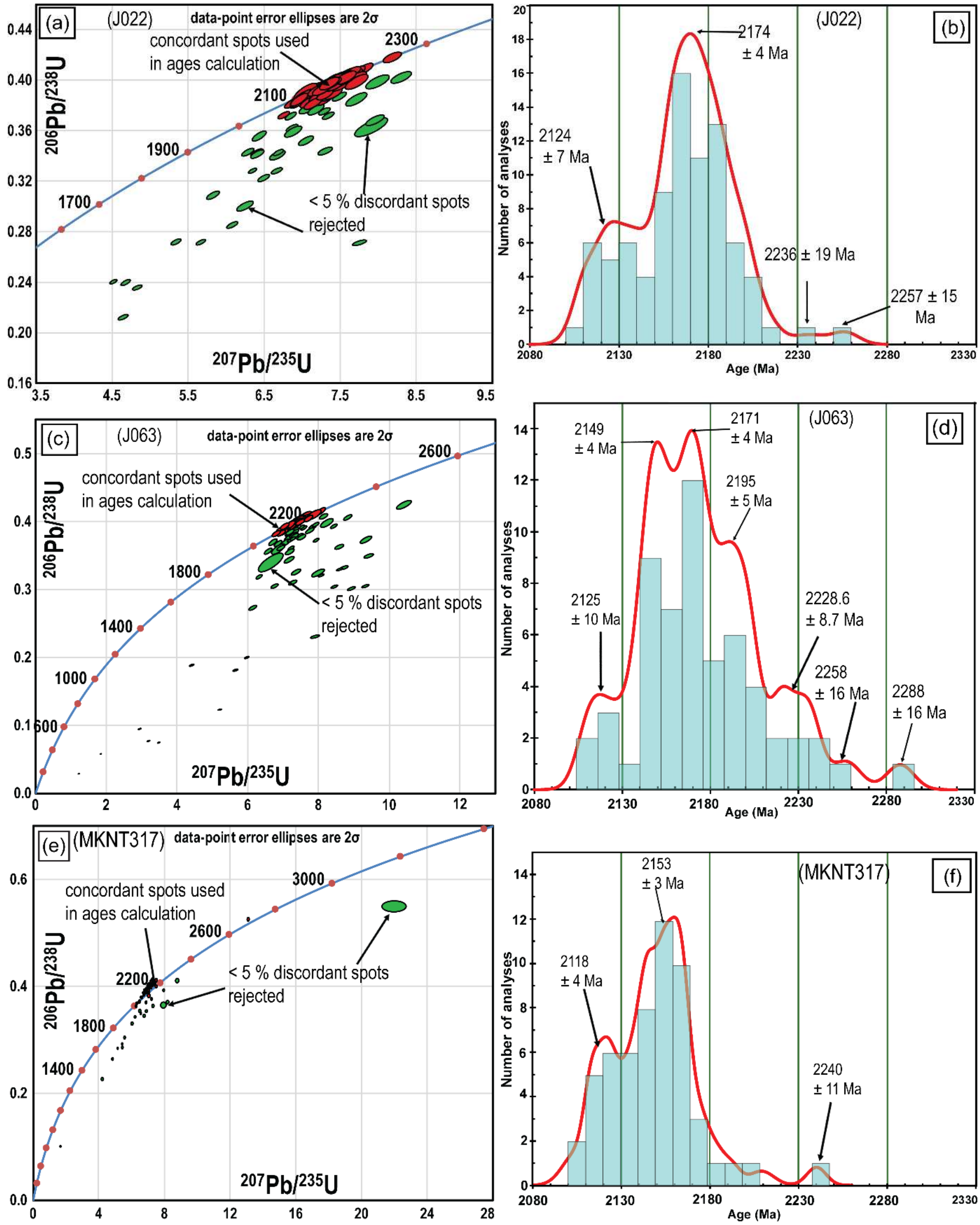
(a)
(J022)
data-point error ellipses are 2σ
concordant spots used in ages calculation
< 5 % discordant spots rejected
$^{206}Pb/^{238}U$
$^{207}Pb/^{235}U$
(b)
(J022)
2174 ± 4 Ma
2124 ± 7 Ma
2236 ± 19 Ma
2257 ± 15 Ma
Number of analyses
Age (Ma)
(c)
(J063)
data-point error ellipses are 2σ
concordant spots used in ages calculation
< 5 % discordant spots rejected
(d)
(J063)
2149 ± 4 Ma
2171 ± 4 Ma
2195 ± 5 Ma
2125 ± 10 Ma
2228.6 ± 8.7 Ma
2258 ± 16 Ma
2288 ± 16 Ma
(e)
(MKNT317)
data-point error ellipses are 2σ
concordant spots used in ages calculation
< 5 % discordant spots rejected
(f)
(MKNT317)
2153 ± 3 Ma
2118 ± 4 Ma
2240 ± 11 Ma

Figure 4.

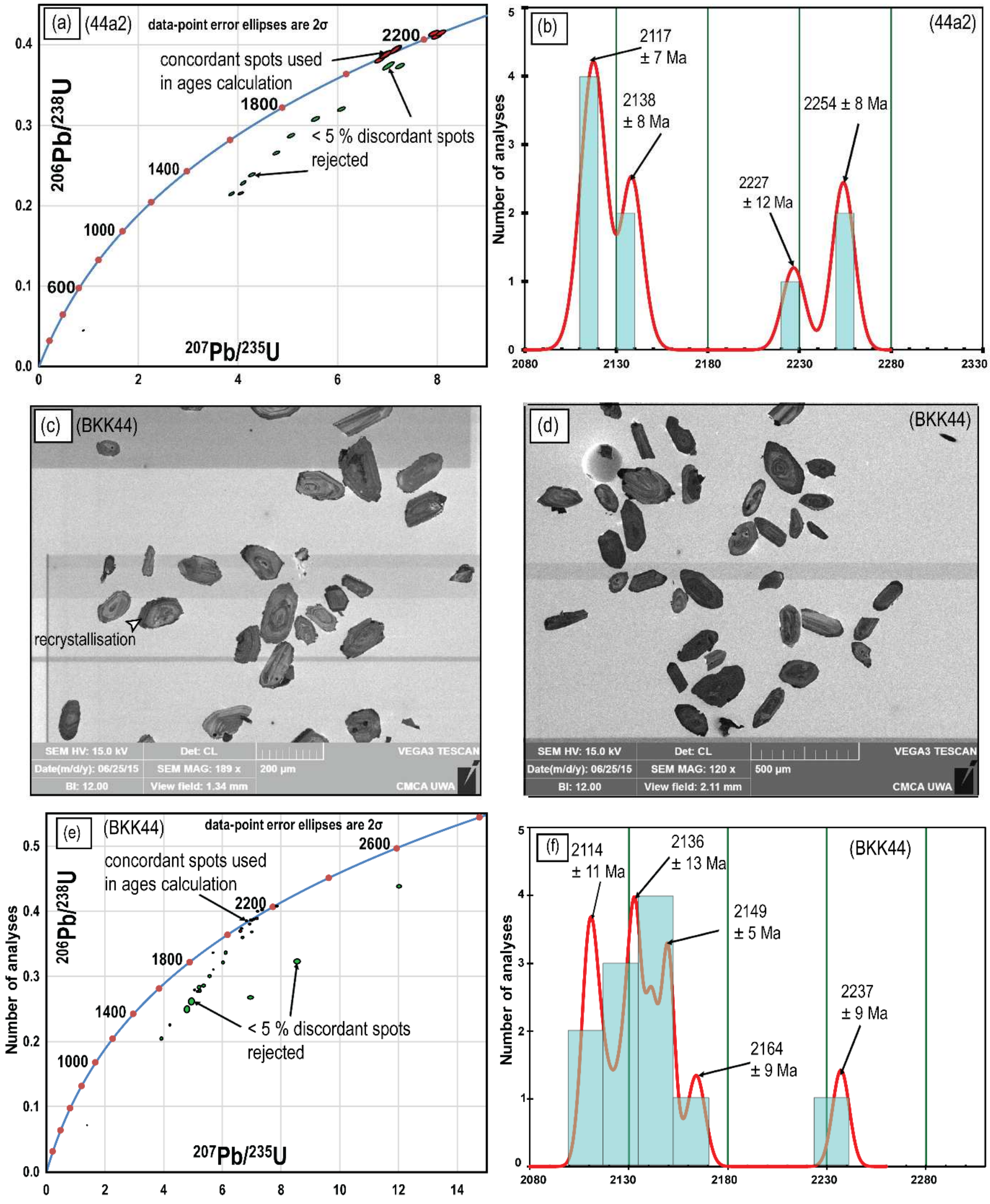
(a) (44a2)
data-point error ellipses are 2σ
concordant spots used in ages calculation
< 5 % discordant spots rejected
^{206}Pb/^{238}U
^{207}Pb/^{235}U
(b) (44a2)
2117 ± 7 Ma
2138 ± 8 Ma
2227 ± 12 Ma
2254 ± 8 Ma
Number of analyses
(c) (BKK44)
recrystallisation
(d) (BKK44)
(e) (BKK44)
data-point error ellipses are 2σ
concordant spots used in ages calculation
< 5 % discordant spots rejected
Number of analyses
^{206}Pb/^{238}U
^{207}Pb/^{235}U
(f) (BKK44)
2114 ± 11 Ma
2136 ± 13 Ma
2149 ± 5 Ma
2164 ± 9 Ma
2237 ± 9 Ma
Number of analyses

Figure 5

	Pb	Th	U	Th/U	208Pb/	207Pb/	±	207Pb/	±	206Pb/	±	Rho	Apparent ages (Ma) 206Pb/	±	207Pb/	±	Disc.
MKNT317-75.d	467	31	132	0.24	0.13	0.1403	0.00105	7.480	0.06	0.3863	0.0029	0.05	2103	14	2209	14	5
MKNT317-39.d	330	34	108	0.31	0.12	0.1423	0.0009	7.910	0.0485	0.4035	0.0023	0.05	2183	11	2240	11	3
MKNT317-06.d	1763	130	495	0.26	0.11	0.18454	0.00065	13.382	0.06	0.5249	0.00255	0.04	2717	11	2691.3	6	-1
MKNT317-52.d	720	73	269	0.27	0.11	0.13508	0.0006	6.949	0.036	0.3728	0.00195	0.05	2040	9	2155	8	6
MKNT317-58.d	547	54	149	0.36	0.14	0.1394	0.0007	7.278	0.041	0.3795	0.00205	0.05	2072	10	2207	9	7
MKNT317-11.d	449	43	147	0.29	0.12	0.147	0.0008	8.017	0.0465	0.3954	0.0019	0.04	2146.8	9	2296	10	8
MKNT317-60.d	521	33	163	0.20	0.14	0.155	0.0013	8.830	0.075	0.4129	0.003	0.04	2222	14	2381	15	8
MKNT317-61.d	330	33	140	0.23	0.10	0.1334	0.00105	6.569	0.055	0.3573	0.00265	0.05	1967	13	2125	14	8
MKNT317-13.d	518	60	250	0.24	0.09	0.1314	0.0006	6.267	0.0325	0.3465	0.0017	0.05	1918.3	8	2109	8	10
MKNT317-08.d	903	94	267	0.35	0.15	0.13594	0.00055	6.613	0.032	0.3527	0.00175	0.05	1945.8	8	2169	7	12
MKNT317-70.d	648	52	160	0.33	0.16	0.1458	0.001	7.350	0.06	0.3661	0.0024	0.04	2007	12	2273	12	13
MKNT317-36.d	526	60	169	0.35	0.13	0.1412	0.0007	6.957	0.042	0.3566	0.0022	0.05	1962	11	2231	9	14
MKNT317-04.d	464	57	233	0.24	0.10	0.1318	0.0006	6.092	0.044	0.334	0.0023	0.05	1852	11	2113	8	14
MKNT317-68.d	145	13	44	0.30	0.14	0.1424	0.00115	6.830	0.055	0.3485	0.0024	0.04	1923	12	2217	14	15
MKNT317-12.d	373	42	64	0.66	0.25	0.1609	0.00155	8.250	0.075	0.3736	0.0025	0.03	2043	12	2434	17	19
MKNT317-45.d	394	59	111	0.53	0.14	0.1581	0.00265	7.990	0.135	0.368	0.0043	0.03	2019	21	2430	27	20
MKNT317-39.d	2710	60	144	0.42	0.47	0.284	0.0055	22.000	0.6	0.55	0.0085	0.01	2818	35	3371	31	20
MKNT317-35.d	551	64	273	0.23	0.10	0.13179	0.0006	5.633	0.0345	0.3081	0.00185	0.05	1732	9	2111	8	20
MKNT317-20.d	768	97	339	0.29	0.12	0.1341	0.00065	5.483	0.0335	0.2967	0.0017	0.05	1673	9	2143	8	25
MKNT317-05.d	572	78	291	0.27	0.11	0.13108	0.0006	5.224	0.031	0.2882	0.0016	0.05	1632	8	2103	8	25
MKNT317-19.d	549	128	249	0.51	0.12	0.138	0.00065	5.517	0.0415	0.2898	0.0022	0.05	1635	11	2190	9	28
MKNT317-14.d	1385	199	339	0.59	0.25	0.13266	0.00055	4.917	0.0405	0.2685	0.0021	0.05	1527	11	2125	8	31
MKNT317-22.d	863	166	355	0.47	0.16	0.1344	0.0007	4.280	0.0485	0.2314	0.0023	0.05	1335	12	2142	9	41
MKNT317-24.d	1196	407	585	0.69	0.30	0.1166	0.00065	1.752	0.024	0.107	0.00125	0.05	652	8	1889	10	69

(44a2) spot	(ppm)	(ppm)	(ppm)		206Pb	206Pb	(1σ)	235U	(1σ)	238U	(1σ)		238U	(1σ)	206Pb	(1σ)	%
jf_27	174	116	375	0.31	0.18	0.1422	0.0010	8.010	0.078	0.409	0.003	0.69	2209	13	2254	12	2.0
jf_28	138	66	307	0.21	0.13	0.1422	0.0010	8.090	0.079	0.413	0.003	0.69	2227	13	2254	12	1.2
jf_29	118	56	262	0.21	0.13	0.1400	0.0010	7.947	0.079	0.412	0.003	0.69	2223	13	2227	12	0.2
jf_36	73	56	162	0.35	0.22	0.1314	0.0011	7.014	0.086	0.387	0.003	0.70	2110	15	2116	15	0.3
jf_38	108	64	257	0.25	0.15	0.1314	0.0010	6.885	0.079	0.380	0.003	0.74	2076	15	2117	13	1.9
jf_39	103	81	226	0.36	0.21	0.1331	0.0010	7.207	0.088	0.393	0.004	0.78	2135	17	2140	13	0.2
jf_42	96	60	214	0.28	0.18	0.1315	0.0012	6.990	0.087	0.386	0.003	0.70	2102	16	2118	16	0.8
jf_43	47	13	116	0.11	0.07	0.1315	0.0009	7.009	0.085	0.387	0.004	0.82	2107	18	2118	12	0.5
jf_45	63	41	141	0.29	0.18	0.1330	0.0008	7.192	0.079	0.392	0.004	0.83	2133	17	2138	11	0.2
jf_44	**55**	**22**	**138**	**0.16**	**0.10**	**0.1363**	**0.0009**	**7.025**	**0.088**	**0.374**	**0.004**	**0.85**	**2047**	**19**	**2181**	**12**	**6.1**
jf_26	**157**	**111**	**371**	**0.30**	**0.18**	**0.1408**	**0.0010**	**7.255**	**0.068**	**0.374**	**0.002**	**0.69**	**2047**	**11**	**2237**	**12**	**8.5**
jf_40	**128**	**143**	**350**	**0.41**	**0.24**	**0.1308**	**0.0011**	**5.565**	**0.066**	**0.309**	**0.002**	**0.68**	**1734**	**12**	**2108**	**15**	**17.7**
jf_30	**162**	**104**	**461**	**0.22**	**0.13**	**0.1375**	**0.0010**	**6.083**	**0.058**	**0.321**	**0.002**	**0.68**	**1795**	**10**	**2195**	**12**	**18.3**
jf_37	**113**	**91**	**356**	**0.26**	**0.15**	**0.1276**	**0.0010**	**5.074**	**0.055**	**0.288**	**0.002**	**0.67**	**1633**	**11**	**2065**	**14**	**20.9**
jf_32	**115**	**180**	**362**	**0.50**	**0.25**	**0.1298**	**0.0010**	**4.782**	**0.050**	**0.267**	**0.002**	**0.68**	**1526**	**10**	**2096**	**13**	**27.2**
jf_41	**98**	**155**	**345**	**0.45**	**0.24**	**0.1295**	**0.0012**	**4.295**	**0.052**	**0.241**	**0.002**	**0.67**	**1390**	**10**	**2091**	**16**	**33.5**
jf_33	**130**	**250**	**449**	**0.56**	**0.33**	**0.1296**	**0.0009**	**4.117**	**0.045**	**0.230**	**0.002**	**0.76**	**1336**	**10**	**2093**	**12**	**36.1**
jf_34	**108**	**197**	**407**	**0.48**	**0.29**	**0.1301**	**0.0009**	**3.887**	**0.043**	**0.217**	**0.002**	**0.77**	**1264**	**10**	**2100**	**12**	**39.8**
jf_31	**111**	**184**	**431**	**0.43**	**0.23**	**0.1355**	**0.0010**	**4.064**	**0.042**	**0.218**	**0.002**	**0.68**	**1269**	**8**	**2170**	**13**	**41.5**
jf_35	**75**	**767**	**1003**	**0.77**	**0.62**	**0.1344**	**0.0008**	**0.915**	**0.010**	**0.049**	**0.000**	**0.82**	**311**	**3**	**2156**	**11**	**85.6**

													Apparent ages (Ma)				
(BKK44) spot	Pb (ppm)	Th (ppm)	U (ppm)	Th/U	208Pb/ 206Pb	207Pb/ 206Pb	± (1σ)	207Pb/ 235U	± (1σ)	206Pb/ 238U	± (1σ)	Rho	206Pb/ 238U	± (1σ)	207Pb/ 206Pb	± (1σ)	Disc. %
BKK44-02.d	326.5	33.44	121.6	0.28	0.115741	0.1335	0.0008	6.769	0.038	0.3704	0.0014	0.037	2030	7	2127	11	5
BKK44-03.d	344.9	32.55	73	0.45	0.175747	0.1353	0.0007	7.493	0.0345	0.4021	0.0011	0.032	2177	5	2148	9	-2
BKK44-04.d	233.1	21.75	149.8	0.15	0.060938	0.1334	0.0006	7.338	0.0305	0.4002	0.001	0.033	2170.2	5	2131	8	-2
BKK44-10.d	657	61.2	163.3	0.37	0.15873	0.13473	0.000475	7.226	0.0275	0.3883	0.00105	0.038	2115	5	2150	6	2
BKK44-14.d	975	97.5	173.9	0.56	0.23663	0.1316	0.00065	6.975	0.0325	0.3861	0.00105	0.032	2104.7	5	2110	9	0
BKK44-17.d	208.4	22.58	62.58	0.36	0.142674	0.1328	0.0007	7.13	0.035	0.387	0.00115	0.033	2107	6	2116	10	0
BKK44-19.d	266.9	29.95	116.58	0.26	0.100503	0.1357	0.0007	7.315	0.0365	0.3896	0.00115	0.032	2120	6	2164	9	2
BKK44-20.d	505	57.2	212.4	0.27	0.097466	0.13387	0.00048	7.079	0.024	0.3812	0.0009	0.038	2080.7	4	2141	6	3
BKK44-27.d	351.9	36.9	161.9	0.23	0.091075	0.1417	0.0007	7.988	0.037	0.4078	0.00115	0.031	2204	6	2237	9	2

Journal Pre-proof

BKK44-24.d	426.1	47.99	195	0.25	0.09646	0.13343	0.00047	7.161	0.0235	0.3867	0.0008	0.034	2107.2	4	2134	6	1
BKK44-25.d	231.3	26.74	239.2	0.11	0.044683	0.1314	0.00055	6.817	0.0255	0.3745	0.00085	0.033	2050.1	4	2110	8	3
BKK44-16.d	**460**	**78.6**	**278.2**	**0.28**	**0.082237**	**0.12182**	**0.000415**	**5.708**	**0.019**	**0.3381**	**0.0008**	**0.042**	**1876.6**	**4**	**1978**	**6**	**6**
BKK44-18.d	**466.3**	**52.31**	**278.8**	**0.19**	**0.07734**	**0.1338**	**0.00065**	**6.708**	**0.031**	**0.3611**	**0.00115**	**0.037**	**1987**	**6**	**2142**	**9**	**8**
BKK44-13.d	**726**	**70.8**	**250.6**	**0.28**	**0.121507**	**0.13809**	**0.000465**	**7.022**	**0.0245**	**0.3693**	**0.0011**	**0.045**	**2025**	**6**	**2198**	**6**	**9**
BKK44-11.d	**1557**	**155.7**	**286.8**	**0.54**	**0.259134**	**0.1324**	**0.0006**	**6.135**	**0.0325**	**0.3381**	**0.0017**	**0.052**	**1876**	**8**	**2124**	**8**	**13**
BKK44-31.d	**249**	**22.2**	**506.5**	**0.04**	**0.024155**	**0.1357**	**0.0007**	**6.046**	**0.0355**	**0.3235**	**0.0015**	**0.042**	**1808**	**8**	**2170**	**9**	**19**
BKK44-09.d	**497**	**36.4**	**206**	**0.18**	**0.076982**	**0.1986**	**0.0006**	**12.03**	**0.07**	**0.4384**	**0.00225**	**0.032**	**2337**	**10**	**2809**	**5**	**20**
BKK44-21.d	**611.8**	**80.9**	**462.1**	**0.18**	**0.074349**	**0.13221**	**0.00046**	**5.716**	**0.0195**	**0.3126**	**0.0007**	**0.036**	**1753.3**	**3**	**2123**	**6**	**20**
BKK44-08.d	**735**	**73.9**	**350**	**0.21**	**0.11274**	**0.1345**	**0.00065**	**5.59**	**0.0385**	**0.3028**	**0.00175**	**0.045**	**1703**	**9**	**2151**	**9**	**24**
BKK44-05.d	**661**	**99**	**298.3**	**0.33**	**0.126103**	**0.1334**	**0.0007**	**5.229**	**0.0425**	**0.2858**	**0.00215**	**0.051**	**1618**	**11**	**2135**	**9**	**27**
BKK44-28.d	**615**	**94.1**	**480.6**	**0.20**	**0.079872**	**0.1307**	**0.0006**	**5.078**	**0.0225**	**0.282**	**0.0008**	**0.036**	**1601.3**	**4**	**2100**	**8**	**27**
BKK44-15.d	**249**	**21.9**	**284**	**0.08**	**0.051921**	**0.1354**	**0.00115**	**5.38**	**0.05**	**0.2884**	**0.00175**	**0.035**	**1632**	**9**	**2168**	**15**	**28**
BKK44-23.d	**732**	**126.6**	**339**	**0.37**	**0.130548**	**0.13507**	**0.000425**	**5.263**	**0.0335**	**0.2804**	**0.0017**	**0.051**	**1589**	**9**	**2158**	**6**	**29**
BKK44-30.d	**358**	**45.9**	**354.7**	**0.13**	**0.059488**	**0.1338**	**0.00075**	**5.178**	**0.0275**	**0.2795**	**0.00095**	**0.035**	**1588.2**	**5**	**2140**	**10**	**29**
BKK44-29.d	**448**	**47.1**	**290.5**	**0.16**	**0.105708**	**0.1373**	**0.0008**	**4.97**	**0.075**	**0.2646**	**0.0042**	**0.056**	**1503**	**21**	**2182**	**10**	**34**
BKK44-07.d	**646**	**60**	**296.6**	**0.20**	**0.125628**	**0.1388**	**0.00055**	**4.82**	**0.075**	**0.2526**	**0.0041**	**0.055**	**1431**	**21**	**2204**	**7**	**38**
BKK44-12.d	**500**	**38.8**	**215.1**	**0.18**	**0.113507**	**0.1894**	**0.0007**	**8.56**	**0.085**	**0.3249**	**0.0028**	**0.033**	**1801**	**14**	**2731**	**6**	**38**
BKK44-26.d	**466**	**75.2**	**502**	**0.15**	**0.070771**	**0.13368**	**0.000495**	**4.241**	**0.025**	**0.2288**	**0.00125**	**0.050**	**1326**	**7**	**2146**	**7**	**42**
BKK44-22.d	**451**	**67.1**	**453.8**	**0.15**	**0.062735**	**0.1874**	**0.00115**	**6.98**	**0.075**	**0.2702**	**0.002**	**0.027**	**1540**	**10**	**2713**	**10**	**48**
BKK44-01.d	**303.2**	**32.7**	**168.5**	**0.19**	**0.129634**	**0.1379**	**0.00065**	**3.947**	**0.0345**	**0.2084**	**0.00185**	**0.054**	**1213**	**10**	**2185**	**8**	**48**
BKK44-06.d	**670**	**212.7**	**1139**	**0.19**	**0.122399**	**0.1339**	**0.00055**	**1.433**	**0.0065**	**0.07761**	**0.00024**	**0.037**	**481.8**	**1**	**2143**	**8**	**80**

The youngest age peaks constrain the maximum deposition age of the Dialé-Daléma series at 2125 ± 10 Ma in the west to ca 2114 ± 11 Ma in the east.